Master's Thesis

Pattern formation in a generalized Klausmeier-Gray-Scott model

Defended on August 23rd 2012

Author:
Lotte Sewalt

Supervisors:
Dr. V. Rottschäfer
Prof. Dr. A. Doelman

Contents

Chapter 1

Introduction

Ever since the Age of Enlightenment in the 18$^{\text{th}}$ century, both intellectuals and amateurs have tried to understand the laws of nature. And even though many answers have been provided by models such as Newton's laws, more questions usually arise during the process. In applied sciences, one of the most challenging tasks is to formulate mathematical models that can describe natural phenomena in a proper manner. These phenomena could vary from the formation of stripe patterns on the skin of African mammals to oceanic currents and the formation of clouds and rivers. The purpose of these models has always been to provide insight in the behavior and perhaps give predictions on the future. However, many complex natural systems are only partly understood so far. One could think about models that are used to describe the future state of the global climate and the difficulties associated with it.

In this thesis, a model describing the balance between vegetation and precipitation in semi-arid ecosystems[1] is considered. At the edge of the deserts, vegetation often occurs in patterns, including stripe-like patterns called tiger bushes. This was observed on aerial photographs in the 1950s [8], see figure 1.1.

Approximately 30% of the emerged surface of the earth is covered with these patterns, in North- and South-America, Africa and Australia. Between shrubs, grass, bushes or trees empty spaces appear at regular intervals.
On hillsides, strips of vegetation alternate with strips of bare ground in a direction parallel to the hill's contours. On flat ground, a wide diversity of stationary patterns occurs. In this thesis, the strips of vegetation on a hillside will be in the center of attention. A striking feature of these strips is that they climb uphill as time passes. The verbal explanation for the persistence and movement of these strips is as follows. In the bare areas, water doesn't infiltrate the soil, but it flows downhill to the first strip of vegetation where it can be taken up. This water is then exhausted upon reaching the downhill side of the strip, which causes again a bare area. This also explains a most striking feature of this pattern formation: the strips slowly move uphill. This is because of the fact that vegetation can grow and survive at the top area of a vegetation strip, because there is enough moisture. On the other hand, the vegetation dies at the bottom area of a vegetation strip, because it is not moist enough [7]. Due to drought, many deserts are expanding. Patterns are an indication of this desertification of the region. The aim of studying this particular phenomenon is therefore to be able to give early warning signals in areas which are directly threatened by desertification. Both ecologists and mathematicians have analyzed models trying to describe and understand the patterns. The first attempts have led to linear Turing patterns and numerical simulations only. However, Van der Stelt [10] was able to perform a specific mathematical analysis in which these patterns were captured.

It is confirmed widely that semi-arid ecosystems in which vegetation patterns occur run the risk of a sudden collapse where the area turns into a desert or dry steppe when a determinant crosses a threshold value. In particular this can be caused by

[1] Ecosystems with an annual precipitation of 250-500 mm are known as semi-arid.

Figure 1.1: Two examples of vegetation patterns found with Google Earth. On the left a vegetation patterns near W National Park in Niger. On the right, a variety of patterns near Zamarkoy in the Sahel desert in Burkina Faso. The vegetation appears in dark while the sand colored pieces are bare soil.

a low rainfall or a high grazing pressure by cattle. The most important feature of this collapse is that it is irreversible. When a vegetated area has been turned into a desert after years of severe drought, it cannot turn into a vegetated area again as the rainfall increases. Therefore, ecologists tend to speak of a catastrophe when this happens.

1.1 Model description

In 1999, C.A. Klausmeier was the first to model the dynamic interplay between water infiltration and vegetation density by a reaction-(advection-)diffusion system [7]. In this model both the periodic patterns as well as the catastrophe described above are captured. A two-component system with water infiltration u and vegetation density v was introduced, reading as follows:

$$\begin{cases} u_t &= k_0 u_x + k_1 - k_2 u - k_3 k_5 u v^2, \\ v_t &= d_v v_{xx} - k_4 v + k_5 u v^2. \end{cases} \tag{1.1}$$

Here $u(x,t), v(x,t) : \mathbb{R} \times \mathbb{R}_+ \to \mathbb{R}$ and $k_i \geq 0, i = 1, \ldots, 5$, $d_v \geq 0$. The first equation of the system describes the change of water infiltration per time unit. It is assumed to be governed by advection caused by the gradient of the slope of the area, $k_0 u_x$, a constant precipitation rate k_1, a linear evaporation rate $-k_2 u$ and the infiltration feedback[2], modeled by $-k_3 k_5 u v^2$. The change in vegetation density per unit of time is modeled by a diffusive spread of biomass, $d_v v_{xx}$, a linear natural death rate $-k_4 v$ and the infiltration feedback $k_5 u v^2$, which of course has a positive effect on the vegetation[3]. It is natural to assume $d_v \ll k_0$ because the spread of biomass occurs on a much slower timescale than the advection of the water.

Remark 1. In [7], the model is actually assumed to be two-dimensional in space, different from (1.1). In this thesis it is assumed that there is a constant variation in the direction of one spatial variable, causing the dynamics to be one-dimensional in space. Also, Klausmeier considered a bounded domain, and here both u and v vary on an infinite domain $\mathbb{R}$. This can be validated by the fact that the scale of the patterns is relatively small compared to the size of the domain. ◀

[2] With the infiltration feedback the uptake of water by the vegetation is meant.
[3] Roughly speaking: the uptake of water gives growth of the vegetation.

The shortcoming in the Klausmeier model is that it assumes the existence of a slope in the area. However, the patterns were observed in both flat and sloping areas. This motivates the following extension of (1.1). The spread of water on a terrain without a specific preference for the direction in which the water flows is modeled as a porous media flow. This yields:

$$\begin{cases} u_t &= d_u(u^\gamma)_{xx} + k_0 u_x + k_1 - k_2 u - k_3 k_5 u v^2, \\ v_t &= d_v v_{xx} - k_4 v + k_5 u v^2. \end{cases} \tag{1.2}$$

Where it is assumed that $\gamma \geq 1$, see [10]. Now there is a diffusion term for the water as well. Because water of course spreads much faster than biomass, it is natural to assume $0 < d_v \ll d_u$, which gives the system a singular perturbed structure. For ecosystems without a slope, $k_0 = 0$.
The model can be rescaled by setting:

$$U = \frac{k_2}{k_1} u, \quad V = \frac{k_2 k_3}{k_1} v, \quad \bar{t} = \frac{k_1^2 k_5}{k_2^2 k_3} t, \quad \bar{x} = \left[d_u \frac{k_3}{k_5} \left(\frac{k_1}{k_2} \right)^{\gamma - 3} \right]^{-\frac{1}{2}} x.$$

This rescaling is convenient because it reduces the number of parameters, and the following system is obtained:

$$\begin{cases} U_t = (U^\gamma)_{xx} + A(1-U) - UV^2 + CU_x, \\ V_t = \delta^{2\sigma} V_{xx} - BV + UV^2, \end{cases} \tag{1.3}$$

where the bars on t and x are dropped and

$$A = k_2 \frac{k_2^2 k_3}{k_1^2 k_5}, \quad B = k_4 \frac{k_2^2 k_3}{k_1^2 k_5}, \quad C = k_0 \frac{k_2^2 k_3}{k_1^2 k_5} \left[d_u \frac{k_3}{k_5} \left(\frac{k_1}{k_2} \right)^{\gamma - 3} \right]^{-\frac{1}{2}},$$

and

$$\delta^{2\sigma} = \frac{d_v}{d_u} \left(\frac{k_2}{k_1} \right)^{\gamma - 1}, \quad \sigma > 0.$$

We have $0 < \delta \ll 1$ because $0 < d_v \ll d_u$ as noted before. In this thesis, the case where $\gamma = 1, \sigma = 1$ will be studied. This yields the central system:

$$\begin{cases} U_t = U_{xx} + A(1-U) - UV^2 + CU_x, \\ V_t = \delta^2 V_{xx} - BV + UV^2, \end{cases} \tag{1.4}$$

where $A, B, C > 0$ and $0 < \delta \ll 1$.
This system of equations will be referred to as the *Generalized Klausmeier-Gray-Scott model*, shortly GKGS-model, because for $C = 0$ the equation reduces to the Gray-Scott model, see [3]. The scalings were chosen according to the characteristics of the ecosystem. The rate of the slope of the terrain is modeled by parameter C, where $C = 0$ corresponds to no slope. Parameter A measures the rainfall and parameter B describes the extinction rate of the biomass.

1.2 Outline

In this thesis, the aim is to construct and analyze solutions of the generalized Klausmeier-Gray-Scott system. The focus will be on the spatially periodic patterns climbing uphill which were observed and described in [7], similar to figure 1.1. These patterns will now be referred to as *traveling patterns*. A guidebook for this

analysis, especially for the first chapters, will be [3]. Also, the geometric approach and Poincaré maps in [5] generated a lot of inspiration, especially for Chapter 5.

In Chapter 2, a traveling wave ansatz will be introduced. This assumes one variable describing both the spatial and the temporal behavior. This reduces the system of PDEs to a system of ODEs. Also, the split analysis in multiple scales arises naturally from here. This chapter forms the foundation for the rest of the thesis. It also includes a section on a rescaling which was motivated by mathematical considerations. This allows us to perform an analysis similar to [3]. The multiple scales imply two reduced systems describing the slow and fast behavior separately to leading order. Fenichel's first theorem will be applied to show persistence of this behavior. In this chapter the overview of geometric singular perturbation theory described in [6] was used.

The onset of the thesis is extended even further in Chapter 3, where the leading order dynamics of the system is studied. The slow and fast behavior are analyzed separately and again Fenichel theory is applied to obtain regularity. In order to find traveling patterns it is sensible to construct a traveling homoclinic pulse first. In this chapter, the first steps towards this construction are described. A saddle type equilibrium P is examined and the leading order descriptions of its stable and unstable manifold are computed.
Moreover, with a Melnikov method [5] and asymptotic expansions of the solutions, the take-off and touch-down curves of the system are computed. This was never done before for this system. The procedure was similar to [2] and [3].

In the fourth chapter, the homoclinic orbit will be constructed. Here the geometric character of the analysis in the thesis starts. A condition for the existence of patterns with a slow/fast structure will be derived. The results are presented in Theorem 4, which will be proved by studying the intersection of the stable and unstable manifold of the equilibrium P. This is a very meticulous job, but the gain is that in this way the existence of a traveling homoclinic orbit is guaranteed. We also determined for which parameter values this homoclinic orbit can exist and what its traveling speed must be.

In Chapter 5, the study of the homoclinic orbit will be expanded to traveling periodic orbits. The approach of [3] is not very convenient to apply on (1.4), becaus (1.4) lacks symmetry properties that the sysstem examined in [3] has. This problem is overcome by using a geometric approach. It uses the definition of a Poincaré map. By showing that this map is a contraction, Banach's fixed point theorem yields a periodic orbit. This method is based on methods in [5]. The result of this procedure is that a sufficient and necessary condition for the existence of periodic orbits is obtained, formulated in Theorem 7 and Lemma 1. A bifurcation curve represents the transition of the situation where no periodic orbits can exist to a situation where there is a periodic orbit for every combination of parameters value. The approach we take here has never been followed.

Chapter 2

Set-up

In this chapter the first manipulations of (1.4) will be made, in order to obtain a rescaled version of the system. The main motivation for this is to alter the system in such a way that well-known methods can be applied to it. For example the methods used in [3], [2] and [6] including the multiple scales approach. The systems for which this *geometric singular perturbation theory* is applied are sometimes referred to as *nearly integrable*. Moreover, in this section we will restrict the system in such a way that it can only describe traveling wave solutions. This is a natural choice considering the solutions that were observed by Klausmeier have this structure.

2.1 Multiple scales

As mentioned before, the focus of attention will be at the phenomenon that strips of vegetation climb uphill. In the one-dimensional system (1.4), this corresponds to traveling pulses in the longitudinal direction (i.e. along the hillside). This means that it is assumed that this pulse does not vary in the direction transversal to the hillside. A natural way to describe this behavior mathematically is as a traveling wave. Therefore it is assumed that a new variable combining both x and t can be used, i.e. $U(x,t) = u(x - St)$ and $V(x,t) = v(x - St)$. Here S denotes the wave speed and hence $S = 0$ corresponds to a stationary state. When this is substituted into (1.4), one obtains:

$$\begin{aligned} u_X &= p, \\ p_X &= uv^2 - (C+S)p - A(1-u), \\ \delta v_X &= q, \\ \delta q_X &= Bv - uv^2 - Sq. \end{aligned} \tag{2.1}$$

Here $X = x - St$ is a new variable. This simplifies (1.4) a little because the system is now reduced to a system of ordinary differential equations. This provides the starting point that was used in [6]. Next introduce a new scale $\hat{X} = \frac{X}{\delta}$. Because δ is a small parameter, $0 < \delta \ll 1$ this is a larger or 'faster' scale.

$$\begin{aligned} u_{\hat{X}} &= \delta p, \\ p_{\hat{X}} &= \delta \left[uv^2 - (C+S)p - A(1-u) \right], \\ v_{\hat{X}} &= q, \\ q_{\hat{X}} &= Bv - uv^2 - Sq. \end{aligned} \tag{2.2}$$

The two systems that were obtained, will be be referred to as the slow (2.1) and fast (2.2) system. They both describe the system (1.4) in the two scales it induces naturally. Because δ is a small parameter, it is natural to study the behavior in the limit for δ approaching zero. This yields a leading order approximation to (1.4) in two scales.

In (2.1), the limit $\delta \to 0$ yields two differential equations and to algebraic expressions. This means that in the limit, the behavior of this system occurs on a manifold

satisfying these algebraic expressions. This is called the *critical manifold* [6]. The expressions describing it are

$$\begin{aligned} 0 &= q, \\ 0 &= Bv - uv^2 - Sq, \end{aligned} \tag{2.3}$$

and together with the first two equations of (2.1) it is called the reduced slow system.
The critical manifold defined above can be given as any subset of $\mathbb{R}^4$ satisfying equations (2.3). This yields $q = 0$ and either $v = 0$ or $v = B/u$. To apply Fenichel theory, see [6] and [4], the critical manifold needs to be compact and normally hyperbolic, i.e. the eigenvalues of the Jacobian of the reduced slow system need to be bounded away from the imaginary axis. The fixed point $(v, q) = (B/u, 0)$ of (2.1) with $\delta = 0$ is not normally hyperbolic for some regions of the parameter space. The fixed point $(v, q) = (0, 0)$ is a saddle point for all parameter values and is therefore always normally hyperbolic. This means that the critical manifold needs to be a compact subset of $\{u, p, v = 0, q = 0\}$ to satisfy the conditions of the theorems of Fenichel. Since the system has a biological application and there is no such thing as negative rainfall, the critical manifold will be defined as $\mathcal{M}_0 \subset \{u > 0, p, v = 0, q = 0\}$. It can be as large as one wishes and in particular it will be large enough for its purpose. By construction, the manifold is invariant for $\delta = 0$. It follows from Fenichel's first theorem [6],[4] that this persists for $\delta > 0$.

Theorem 1 (Fenichel's first theorem)**.** *Suppose $\mathcal{M}_0 \subset \{q = 0, Bv - uv^2 - Sq = 0\}$ is compact, possibly with boundary, and normally hyperbolic. Suppose the equations describing* (1.4) *are smooth. Then, for $\delta > 0$ and sufficiently small there exists a manifold $\mathcal{M}_\delta$ which is $\mathcal{O}(\delta)$ close to $\mathcal{M}_0$ and diffeomorphic to $\mathcal{M}_0$. Moreover, $\mathcal{M}_\delta$ is locally invariant under the flow of the first two equations of* (2.1)*, meaning that orbits on $\mathcal{M}_\delta$ cannot leave this manifold via the directions perpendicular to it, but only in the slow direction.*

In this case $\mathcal{M}_\delta = \mathcal{M}_0$ because for $\delta > 0$ and $v = q = 0$, $\mathcal{M}_0$ persists to be locally invariant. From now on this *slow manifold*[1] will simply be referred to as $\mathcal{M}$. The behavior on $\mathcal{M}$ is described by the first equation of (2.1) and, hence, by $u_{XX} + (C + S)u_X + A(1 - u) = 0$, having an saddle equilibrium solution at $u = 1, u_X = p = 0$. This equilibrium corresponds to a constant rainfall ($p = 0$) with no vegetation at all (because $v = q = 0$).

These were conclusions that can be drawn from the limit $\delta \to 0$ in (2.1), but something similar can also be done in (2.2). The limit $\delta \to 0$ yields in (2.2) that $u_{\hat{X}} = p_{\hat{X}} = 0$. This means that, considered in the reduced fast system which is obtained by setting $\delta = 0$ in (2.2), these variables are constant to leading order. The determining behavior there is described by $v_{\hat{X}\hat{X}} + Sv_{\hat{X}} - Bv + uv^2 = 0$ where u is treated as a fixed parameter.

The effect of this splitting in slow and fast systems is that solutions of (1.4) consist of slow and fast parts, described by both systems (2.1) and (2.2). A periodic orbit consisting of slow parts in $\mathcal{M}$ and fast excursions is then a periodic traveling pulse solution of (1.4), because it has a rapid change in a fast timescale. This can easily be related to the biological behavior. A high peak in the v-component is related to a strip of vegetation. These strips are surrounded by bare soil so on both sides of it the v-component is zero to leading order. The water infiltration u is lower where the strip is located, because this is where the water will be taken up. The water infiltration u has a larger value where v is almost zero. In this thesis, two kinds of

[1] Because the dynamics on $\mathcal{M}_\delta$ is described by the slow system.

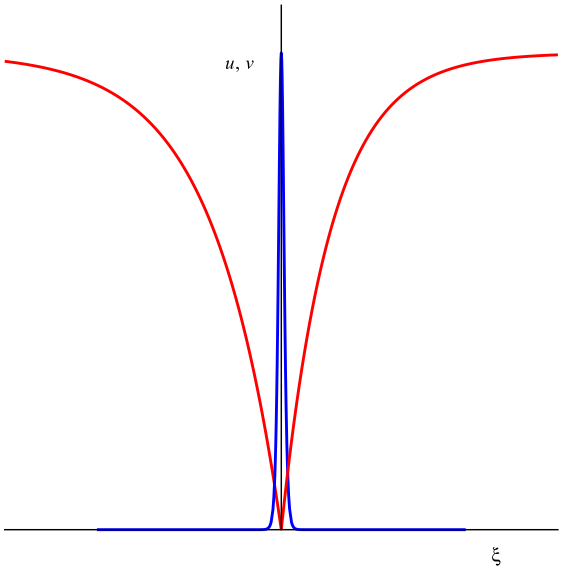

Figure 2.1: Homoclinic traveling pulse solution of system (2.4), which is a rescaled version of (2.1) and (2.2). This pulse corresponds to an oasis. The blue line is the V solution, corresponding to the vegetation. The red line is the U solution, which corresponds to the water. The solution was plotted with $\delta = 0.03$, $\varepsilon = 0.1$, $a = c = 10$ and $s = 1$.

patterns will be analyzed. A single pulse solution, corresponding to a single strip of vegetation or an oasis is considered in Chapter 4, while multiple pulse solutions are examined in Chapter 5. These patterns of interest are plotted in figures 2.1 and 2.2.

2.2 RESCALING

It is not a priori clear that the parameters A, B, C, S in system (1.4) are all $\mathcal{O}(1)$ compared to δ. Therefore, another rescaling is introduced. Several conditions were taken into account in determining the new variables and parameters. First of all, recall that geometric singular perturbation theory is in particular useful in nearly integrable systems. Therefore, the V-equation was rescaled to be integrable at leading order.
Another condition is that the U-equation needs to exhibit slow behavior. This results in a system to which the methods in [2], [3] and [6] can be applied. Also, the rescaling was partly prescribed by biological considerations. For example, the diffusion in U, water, must remain faster than the diffusion in V, vegetation, after rescaling because water diffuses faster than biomass. This all motivates the the rescaling below.

Introduce a new variable

$$\xi = \frac{(x - St)}{\delta\sqrt{\varepsilon}}, \quad S = \delta\varepsilon\sqrt{\varepsilon}s,$$

where it is sensible that S is small, because the velocity of the strips of vegetation is small. Also rescale parameter

$$B = \frac{b}{\varepsilon},$$

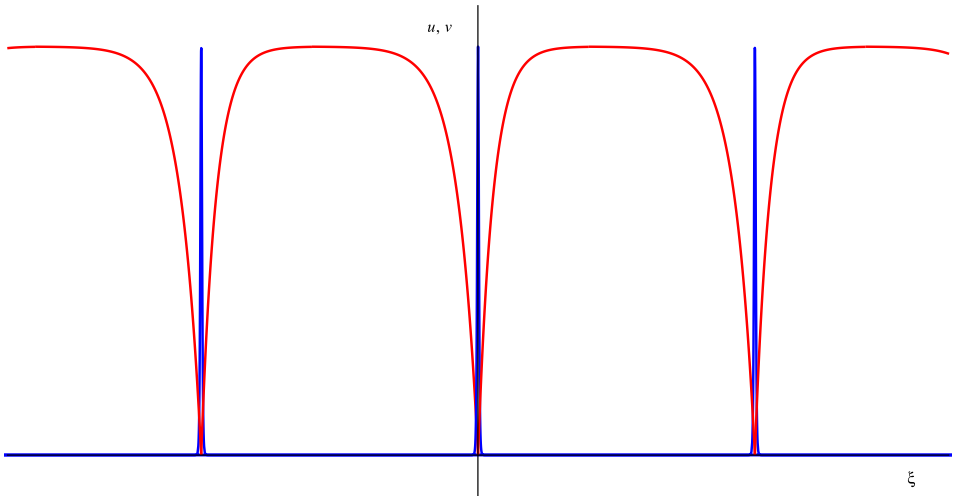

Figure 2.2: Spatially periodic traveling pulse solution of system (2.4), which is a rescaled version of (2.1) and (2.2). This corresponds to a spatially periodic pattern traveling uphill. The blue line is the V solution, the red line is the U solution. The solution was plotted with $\delta = 0.03$, $\varepsilon = 0.1$, $a = c = 10$ and $s = 1$.

and

$$u = \delta\varepsilon\sqrt{\varepsilon}\hat{u}, \quad v = \frac{\sqrt{\varepsilon}}{\delta}\hat{v},$$

where $\varepsilon = \delta^{\frac{1}{\mu}}$ with $\mu > 0$.

Moreover, we will denote $a = A$ and $c = C$. Note that a is still the parameter that controls the rainfall, b is still the decay rate of the plants and c is the slope of the area. In this thesis it is crucial that $s, c \neq 0$, because this indicates the behavior that was not yet studied in [3], even though ecologists did observe the corresponding behavior (i.e. a wave traveling uphill with a nonzero speed).

Substituting the new variables and parameters into (2.1) and with a slight abuse of notation by dropping the hats on u and v, the following system is obtained.

$$\begin{cases} u_\xi = \varepsilon p, \\ p_\xi = \varepsilon\left[uv^2 - a\sqrt{\varepsilon}\delta\left(1 - \dfrac{\delta}{\varepsilon\sqrt{\varepsilon}}u\right)\right] - \sqrt{\varepsilon}\delta p\left(c + s\varepsilon\sqrt{\varepsilon}\delta\right), \\ v_\xi = q, \\ q_\xi = bv - uv^2 - s\varepsilon^2 q. \end{cases} \tag{2.4}$$

This describes again a slow/fast-system with u, p the slow variables and v, q the fast ones. From now on both parameters ε and δ are considered small, i.e. not $\mathcal{O}(1)$.

Chapter 3

Leading order dynamics

In the previous chapter the first step towards a splitting analysis in slow and fast behavior was already set. In this chapter a more detailed analysis will be performed. First, the leading order dynamics of the slow system (2.4) will be studied and then the fast behavior will be considered by rescaling the variable ξ with ε. With this information the so-called take-off and touch-down curves can be determined, which will give insight in how the slow and fast reduced systems can be combined.

3.1 Slow behavior

As was already explained in Chapter 2, to leading order, the slow dynamics is displayed on $\mathcal{M}$ (see the definition in Section 2.1) only. In this section the reduced slow system will be analyzed, i.e. the system restricted to $\mathcal{M}$.

This part of the system gives insight in the behavior of u and p, the water infiltration in the model. Moreover, it corresponds to the region of ξ where v is exponentially small. This means that $\xi = \mathcal{O}(1)$ and not smaller. Later in this section, a new variable $\chi = \varepsilon\xi$ will be introduced, but throughout this thesis, we will mostly work with (2.4), which describes the behavior in a slow (compared to χ) variable ξ. This system is therefore called slow system and for clarity it restated below as (3.1).

$$\begin{aligned} u_\xi &= \varepsilon p, \\ p_\xi &= \varepsilon\left[uv^2 - a\sqrt{\varepsilon}\delta\left(1 - \frac{\delta}{\varepsilon\sqrt{\varepsilon}}u\right)\right] - \sqrt{\varepsilon}\delta p\left(c + s\varepsilon\sqrt{\varepsilon}\delta\right), \\ v_\xi &= q, \\ q_\xi &= bv - uv^2 - s\varepsilon^2 q. \end{aligned} \tag{3.1}$$

Note that on $\mathcal{M}$, the terms including v or q vanish, this gives:

$$\begin{aligned} u_\xi &= \varepsilon p, \\ p_\xi &= \varepsilon\left[-a\sqrt{\varepsilon}\delta\left(1 - \frac{\delta}{\varepsilon\sqrt{\varepsilon}}u\right)\right] - \sqrt{\varepsilon}\delta p\left(c + s\varepsilon\sqrt{\varepsilon}\delta\right), \\ v_\xi &= 0, \\ q_\xi &= 0. \end{aligned} \tag{3.2}$$

The saddle type equilibrium of (2.1) is now rescaled to $P = (u, p, v, q) = (\frac{\varepsilon\sqrt{\varepsilon}}{\delta}, 0, 0, 0)$. Or, when the restricted slow subsystem is considered, $(u, p) = (\frac{\varepsilon\sqrt{\varepsilon}}{\delta}, 0)$. The corresponding Jacobian J with respect to the first two equations of (3.1) is:

$$J\left(\frac{\varepsilon\sqrt{\varepsilon}}{\delta}, 0\right) = \begin{pmatrix} 0 & \varepsilon \\ a\delta^2 & -\sqrt{\varepsilon}\delta(c + s\varepsilon\sqrt{\varepsilon}\delta) \end{pmatrix},$$

where $v = q = 0$ was substituted because the slow behavior is concentrated on $\mathcal{M}$. The manifold $\mathcal{M}$ is invariant under the flow of (2.4). The eigenvalues of the

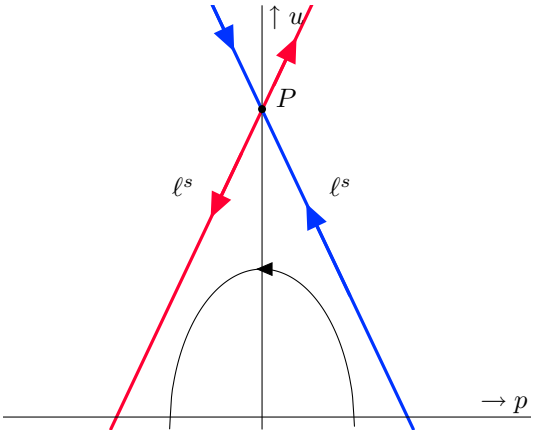

Figure 3.1: Sketch of the slow field described by the first equations of system (3.1). In red, the unstable manifold of P restricted to $\mathcal{M}$ is represented, the blue line is the stable manifold of P. The equilibrium P lies at $(u, p, v, q) = (\varepsilon^{\frac{3}{2}-\mu}, 0, 0, 0)$ which is far away. Hence, the figure is merely a qualitative representation of the dynamics on $\mathcal{M}$.

Jacobian are

$$\begin{aligned}\lambda_\pm &= \frac{1}{2}\left[-\sqrt{\varepsilon}\delta c - s\varepsilon^2\delta^2 \pm \sqrt{\varepsilon\delta^2(c^2 + 2cs\varepsilon\sqrt{\varepsilon}\delta + s^2\varepsilon^3\delta^2 + 4a)}\right], \\ &= \frac{1}{2}\left[-\sqrt{\varepsilon}\delta c - s\varepsilon^2\delta^2 \pm \sqrt{\varepsilon}\delta\sqrt{(c + s\varepsilon\sqrt{\varepsilon}\delta)^2 + 4a)}\right].\end{aligned}$$

Because both eigenvalues are real-valued ($a > 0$) and of the form $\lambda_\pm = -B \pm \sqrt{B^2 + A}$, it is easily verified that there is always both a negative and a positive eigenvalue, which gives this equilibrium a saddle character again. From analysis of the full system (2.4) it follows that the stable and unstable manifolds of P, $W^s(P)$ and $W^u(P)$ are two-dimensional, because there are two positive and two negative eigenvalues. Restricted to the slow manifold $\mathcal{M}$ these are one-dimensional, described by:

$$\ell^{s,u} : \left\{p = \frac{1}{2}\left[-c - s\varepsilon\sqrt{\varepsilon}\delta \pm \sqrt{(c + s\varepsilon\sqrt{\varepsilon}\delta)^2 + 4a}\right]\left(\frac{u\delta}{\sqrt{\varepsilon}} - \varepsilon\right)\right\}, \tag{3.3}$$

where $\ell^s \subset W^s(P)$ corresponds to the $-$ sign and $\ell^u \subset W^u(P)$ corresponds to the $+$ sign. The $\ell^{s,u}$ are depicted in the phase plane in figure 3.1. It will be derived below that the equilibrium P has a large u-value and this phase plane is just a qualitative picture of the behavior on $\mathcal{M}$.

In order to apply methods that were used in [3] it is necessary to choose δ with respect to ε as follows:

$$\delta = \varepsilon^\mu, \text{where} \quad \mu > \frac{3}{2}.$$

The asymptotic methods that will be used later in this chapter can only be applied when ε is small. This automatically yields that δ is even smaller.

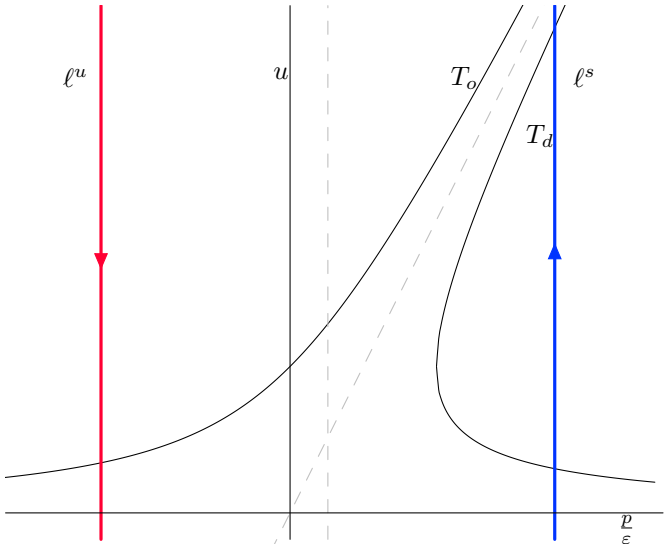

Figure 3.2: Schematic illustration of the slow vector field, the behavior on $\mathcal{M}$. The p-scale is on a $\mathcal{O}(\varepsilon)$ scale and therefore the figure depicts the plane with a vertical zoom. To leading order, the stable and unstable manifold of fixed point P are symmetric around the line $p = c$, indicated with a dashed gray line. The take-off and touch-down curves are symmetric around the line $p = su$, also indicated in gray. The fixed point P has a large u-component and is therefore not present in the picture.

Note that, as a consequence of this choice for δ, the u-value of the saddle point P is 'large'. We have $P = \left(\varepsilon^{\frac{3}{2}-\mu}, 0, 0, 0\right)$. Then, to leading order, the stable and unstable manifolds of P, when restricted to $\mathcal{M}$ become:

$$\ell^{s,u} : \left\{ p = \frac{1}{2}\varepsilon(c \mp \sqrt{c^2 + 4a}) + \mathcal{O}(\varepsilon^{\mu-\frac{1}{2}}) \right\}, \tag{3.4}$$

where now the expression is rewritten such that the one with $+$ sign corresponds to the stable manifold and the $-$ sign to the unstable manifold.

Remark 2. In the expression above, the manifolds $\ell^{s,u}$ are independent of u and hence parallel straight lines in $\mathcal{M}$, which seems counter intuitive because these are the stable and unstable manifolds of P restricted to $\mathcal{M}$; they should by definition intersect in P.
However, this is explained by the fact that (3.4) is a leading order approximation and the u-coordinate of the saddle point is large, $\mathcal{O}(\varepsilon^{\frac{3}{2}-\mu})$. These approximated $\ell^{s,u}$ are depicted in the (u, p)-phase plane in figure 3.2. Here the fixed point P is not depicted, because it is far away from the origin. This means that, with respect to figure 3.1, figure 3.2 is the same but zoomed in around the origin.
Note also, that in the leading order approximation of $\ell^{s,u}$ it was implicitly assumed that $u = \mathcal{O}(1)$. ◀

Because on the slow manifold the equations (3.1) describe the dynamics, and the right hand sides are $\mathcal{O}(\varepsilon)$, it is natural to introduce a new variable $\chi = \varepsilon\xi$ such that we get an $\mathcal{O}(1)$ description of the slow flow. Moreover, on $\mathcal{M}$ it holds that

$v = q = 0$ and $\delta = \varepsilon^\mu$. This yields another rescaled version of the system:

$$\begin{aligned} u' &= p, \\ p' &= -a\varepsilon^{\mu+\frac{1}{2}}\left(1 - \varepsilon^{\mu-\frac{3}{2}}u\right) - \varepsilon^{\mu+\frac{1}{2}}p\left(c + s\varepsilon^{\mu-\frac{3}{2}}\right), \\ \varepsilon v' &= 0, \\ \varepsilon q' &= 0. \end{aligned} \tag{3.5}$$

Where $'$ means differentiation with respect to χ. This displays very well that this is the system describing the slow dynamics. It still exhibits a saddle equilibrium $P = (\varepsilon^{\frac{3}{2}-\mu}, 0)$ and the leading order approximation of the stable and unstable manifolds $\ell^{s,u}$ restricted to $\mathcal{M}$ are given by (3.4).

3.2 Fast behavior

In the previous section, the behavior on $\mathcal{M}$ was described. However, during the fast excursion of the solutions, where v and q become $\mathcal{O}(1)$ and ξ is small, the behavior of (2.4) is dictated by the fast subsystem[1]. This is given by

$$\begin{aligned} v_\xi &= q, \\ q_\xi &= bv - uv^2 - s\varepsilon^2 q. \end{aligned} \tag{3.6}$$

Because $0 < \varepsilon \ll 1$, it is natural to consider the limit $\varepsilon \to 0$ again. For $\varepsilon = 0$, the system (3.6) is Hamiltonian. Its Hamiltonian is given by:

$$K(v, q; u, p) = \frac{1}{2}q^2 - \frac{1}{2}bv^2 + \frac{1}{3}uv^3, \tag{3.7}$$

where u and p are regarded as parameters since u, p are constant in the limit where $\varepsilon \to 0$. System (3.6) possesses a homoclinic solution to the saddle point $(v, q) = (0, 0)$:

$$\begin{aligned} v_0(\xi; u_0) &= \frac{3b}{2u_0}\operatorname{sech}^2\left(\frac{\sqrt{b}}{2}\xi\right), \\ q_0(\xi; u_0) &= \dot{v}_0, \end{aligned} \tag{3.8}$$

where the dot denotes differentiation with respect to ξ.
The reduced fast system also possesses a center equilibrium at $v = \frac{b}{u}, q = 0$. With use of the Hamiltonian K the entire phase plane is easily put together, see figure 3.3. Since the system (2.4) is four-dimensional and the figure is only two-dimensional, the slow manifold $\mathcal{M}$, which is attached to the fast field, is represented as zero-dimensional.

Note that for $\varepsilon = 0$, there exists a solution homoclinic to $\mathcal{M}$ as depicted, for every u, p. There exists a 2-parameter family of homoclinic solutions, parametrized by both u and p, i.e. the plane $\mathcal{M}$. Considered from the fast field perspective, this manifold consists of hyperbolic equilibria. In the case where $\varepsilon = 0$, this corresponds to $\mathcal{M}_0$ having three-dimensional stable and unstable manifolds, $W^s(\mathcal{M}_0)$ and $W^u(\mathcal{M}_0)$, that coincide.
For $\varepsilon > 0$, these manifolds in general no longer coincide, but the manifolds do persist separately. This follows from Fenichel's second theorem, see [6],[4].

[1] It is a subsystem because the first two equations are left out of consideration

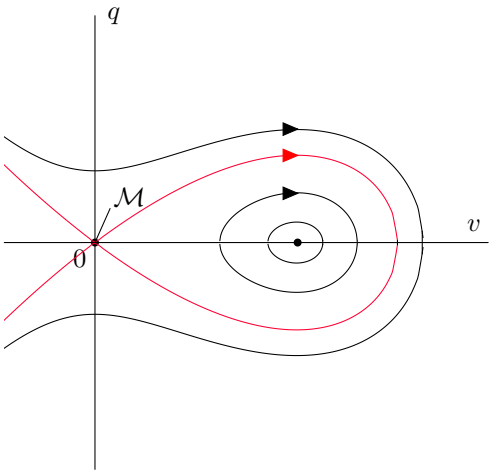

Figure 3.3: Schematic illustration for the fast field. The point $(v, q) = (0, 0)$ represents a two-dimensional manifold $\mathcal{M}$. In red, the solution homoclinic to $\mathcal{M}$ is depicted.

Theorem 2 (Fenichel's second theorem)**.** *Suppose $\mathcal{M}_0 \subset \{q = 0, bv - uv^2 - s\varepsilon^2 q = 0\}$ is compact, possibly with boundary and normally hyperbolic. Suppose the equations describing the flow are smooth. Then for $\varepsilon > 0$ and sufficiently small, there exist manifolds $W^s(\mathcal{M}_\varepsilon)$ and $W^u(\mathcal{M}_\varepsilon)$ that are $\mathcal{O}(\varepsilon)$ close and diffeomorphic to $W^s(\mathcal{M}_0)$ and $W^u(\mathcal{M}_0)$, respectively. Moreover, these manifolds are locally invariant under the flow of* (2.4).

In (2.4), $\mathcal{M}_0 = \mathcal{M}_\varepsilon$. However, this does not indicate that $W^{s,u}(\mathcal{M}_0) = W^{s,u}(\mathcal{M}_\varepsilon)$. Note that in chapter 2 the perturbation was described in terms of δ and here the system is perturbed by ε, this has no qualitative influence on the application of Fenichel's theorems because δ and ε a both small parameters. As mentioned before, when $\varepsilon = 0$, for every point $(u_0, p_0) \in \mathcal{M}_0$ there existed an orbit in the fast reduced system homoclinic to that point. A graphical representation of this is given in figure 3.4. In figure 3.5 a sketch is given of what happens to $W^{s,u}(\mathcal{M}_0)$ for $\varepsilon \neq 0$.

From Fenichel's second theorem, it follows that there can exist a homoclinic orbit to $\mathcal{M}$ for $\varepsilon > 0$, provided that $W^{s,u}(\mathcal{M}_\varepsilon)$ intersect transversally. Under the condition that the manifolds intersect, the homoclinic orbit is displayed in figure 3.5. In that case, the homoclinic orbit to P is a combination of orbits in figures 3.1 and 3.3. In 3.1 one can see that an orbit homoclinic to P must coincide with ℓ^s and ℓ^u represented in blue and red respectively. However, since homoclinic orbits in the fast field could a priori exist for *every* (u, p), every homoclinic orbit in (2.4) will consist of 3 parts. A slow part on $\mathcal{M}$ near ℓ^u, followed by an excursion through the fast field: a homoclinic (to $\mathcal{M}$) orbit in figure 3.3. To return to P, this orbit must get close to ℓ^s, because all other orbits on $\mathcal{M}$ are not attracted by P.

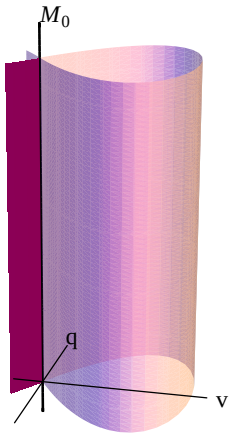

Figure 3.4: Representation of $W^{s,u}(\mathcal{M}_0)$ in three dimensions. The two-dimensional manifold $\mathcal{M}_0$ is reduced to one dimension. The stable and unstable manifold of $\mathcal{M}_0$ coincide and are densely filled with orbits homoclinic to $\mathcal{M}_0$.

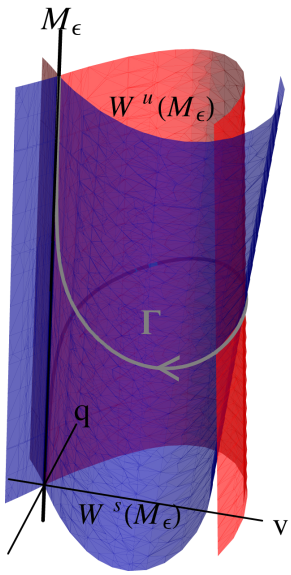

Figure 3.5: Representation of $W^{s,u}(\mathcal{M}_\varepsilon)$ in three dimensions. The two-dimensional manifold $\mathcal{M}_\varepsilon$ is reduced to one dimension. The stable and unstabel manifold of $\mathcal{M}_\varepsilon$ no longer coincide. Fenichel's second theorem assures that these manifolds are still three-dimensional (although they are represented here as two-dimensional) and close to $W^{s,u}(\mathcal{M}_0)$.

3.3 MELNIKOV'S METHOD

One of the prospects for the rest of this thesis is to construct a homoclinic orbit in (2.4). In order to do so, we must find a one-dimensional intersection of the stable and unstable manifolds of P. Because the homoclinic orbit has a slow/fast structure, the fast part of this homoclinic to P orbit must be homoclinic to $\mathcal{M}$ because P is on $\mathcal{M}$.
In the $\varepsilon = 0$ case, this is always possible because the stable and unstable manifolds of $\mathcal{M}$ coincide. For $\varepsilon > 0$ this is no longer the case; the symmetry of the Hamiltonian system (3.6) breaks. Because the stable and unstable manifolds are three-dimensional, there is generally a two-dimensional intersection of the manifolds in $\mathbb{R}^4$. A Melnikov method can be applied to detect this intersection [2] [3] [5]. This method will be performed in this section.

One way to apply Melnikov's method is with the use of the Hamiltonian K, in (3.7). By construction, the hyperplane $\{q = 0\}$ is transverse to $W^s(\mathcal{M}_0)$ and $W^u(\mathcal{M}_0)$. Fenichel's second theorem then explains that $\{q = 0\}$ must also be transverse to both $W^s(\mathcal{M}_\varepsilon)$ and $W^u(\mathcal{M}_\varepsilon)$. This fact will be used in the Melnikov function. Since $W^s(\mathcal{M}_\varepsilon)$ and $W^u(\mathcal{M}_\varepsilon)$ are three-dimensional manifolds, they will intersect with $\{q = 0\}$ transversely in two-dimensional manifolds. Define these manifolds to be parametrized by $(u(0), p(0))$

$$I_\pm(\mathcal{M}) := \{(u(0), p(0), v_\pm(u(0), p(0)), 0); u(0) > 0\} \subset \{q = 0\}.$$

Note that this parametrization is possible because the intersection with $\{q = 0\}$ is transverse. To explain the definition of $I_\pm$ a bit more: for every initial condition in $\mathcal{M}$ there exist $v_\pm$ such that an orbit $\gamma(\xi)$ with initial condition $\gamma(0) = (u(0), p(0), v_-(0), 0)$ has limit $\lim_{\xi\to\infty} \gamma(\xi) \in \mathcal{M}$. Moreover it holds that an orbit $\gamma(\xi)$ with initial condition $\gamma(0) = (u(0), p(0), v_+(0), 0)$ has limit $\lim_{\xi\to-\infty} \gamma(\xi) \in \mathcal{M}$. An transverse intersection of $I_+(\mathcal{M})$ with $I_-(\mathcal{M})$ would immediately deliver an orbit homoclinic to $\mathcal{M}$. This same reasoning was used in [2].

Because in this case it holds that $K \equiv 0$ on $\mathcal{M}_\varepsilon$ the K-value at the intersection with $\{q = 0\}$ can be calculated. This is used as a distance measurement where a distance zero corresponds to a transverse intersection. The measurement is defined as:

$$\Delta K(u_0, p_0) = \int_{I_f} \dot{K}(v, q; u, p) d\xi \tag{3.9}$$

as $\varepsilon \to 0$. Here I_f is the interval in the ξ-scale which represents the fast jump, or, the interval where the fast reduced system is valid. This is an interval $[-\varepsilon^\alpha, \varepsilon^\alpha]$ in the χ scale. It must hold that $\alpha > 0$ because this is considered a 'small' region in χ-scale. For $\varepsilon \to 0$ its boundaries must approach zero in the sense of χ. For ξ this interval is described as $[-\varepsilon^{\alpha-1}, \varepsilon^{\alpha-1}]$ and it must satisfy the property that the interval approaches the real line as $\varepsilon \to 0$. Therefore it must hold that $\alpha < 1$. In this thesis, it will be assumed that $\alpha = \frac{1}{2}$, an arbitrary choice, so in the sense of ξ we find:

$$I_f := \left[-\frac{1}{\sqrt{\varepsilon}}, \frac{1}{\sqrt{\varepsilon}}\right]. \tag{3.10}$$

This interval is also depicted in figure 3.6.

Any orbit of (2.4) that is homoclinic to $\mathcal{M}$ must satisfy the condition

$$\Delta K(u_0, p_0) = \int_{I_f} \dot{K}(v, q; u, p) d\xi = 0.$$

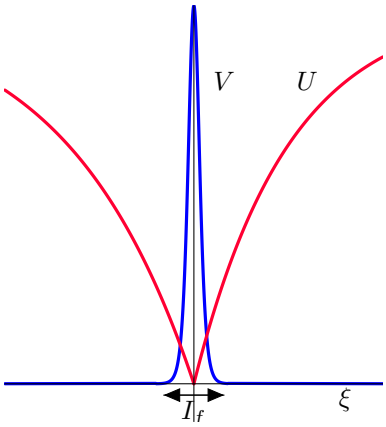

Figure 3.6: Horizontal zoom of figure 2.1. The red line represents the solution for U, the blue represents the solutions for V. The interval $I_f = [-1/\sqrt{\varepsilon}, 1/\sqrt{\varepsilon}]$ is a measure for the width of the V-pulse.

If this zero is simple, the intersection of $W^s(\mathcal{M})$ with $W^u(\mathcal{M})$ is transverse. Since K is known, see (3.7), a straightforward computation yields:

$$\begin{aligned} \dot{K} &= q\dot{q} - bv\dot{v} + \frac{1}{3}\dot{u}v^3 + uv^2\dot{v} \\ &= \frac{1}{3}\varepsilon p v^3 - s\varepsilon^2 q^2. \end{aligned}$$

To determine the integral (3.9) for the perturbed stable and unstable manifolds $W^s(\mathcal{M})$ and $W^u(\mathcal{M})$, an asymptotic method will be used. The asymptotic expansions of $(u(\xi), p(\xi), v(\xi), q(\xi))$ that will be used are in this case in powers of ε. This is a natural choice because ε is the perturbation parameter. Note that the order of the powers of ε depend on the choice of μ. In system (2.4), the terms containing δ are only in the p-equation. It was assumed that $\mu > \frac{3}{2}$, and the terms are ordered in such a way that the expansions remain determined at least up to terms smaller than $\mathcal{O}(\varepsilon^2)$. Note that the higher order terms depend on the specific choice of μ. The expansions that will be used are:

$$\begin{aligned} u(\xi) &= u_0 + \varepsilon u_1(\xi) + \varepsilon^2 u_2(\xi) + \text{ h.o.t.} \\ p(\xi) &= p_0 + \varepsilon p_1(\xi) + \varepsilon^2 p_2(\xi) + \text{ h.o.t.} \\ v(\xi) &= v_0(\xi) + \varepsilon v_1(\xi) + \varepsilon^2 v_2(\xi) + \text{ h.o.t.} \\ p(\xi) &= q_0(\xi) + \varepsilon q_1(\xi) + \varepsilon^2 q_2(\xi) + \text{ h.o.t.} \end{aligned} \tag{3.11}$$

as $\varepsilon \to 0$. Note that for u and p the first terms do not depend on ξ. Also, $v_0(\xi)$ and $q_0(\xi)$ are the homoclinic solutions that were already found for the unperturbed system, see (3.8). This makes sense because in the construction of a homoclinic orbit in the fast field of the perturbed system, the solution will be close to the unperturbed system, where it was derived that u_0 and p_0 were constant.

We asssume $u(0) = u_0$ and $u_j(0) = 0$ for $j \geq 1$. This will set the initial conditions because the other initial conditions will be determined as a function of u_0.

Substitution of (3.11) into (2.4) yields the following:

$$\begin{aligned}
\varepsilon\dot{u}_1(\xi) + \varepsilon^2\dot{u}_2(\xi) + \ldots &= \varepsilon p_0 + \varepsilon^2 p_1(\xi) + \ldots, && (3.12)\\
\varepsilon\dot{p}_1(\xi) + \varepsilon^2\dot{p}_2(\xi) + \ldots &= \varepsilon(u_0 + \varepsilon u_1(\xi) + \ldots)(v_0(\xi) + \varepsilon v_1(\xi) + \ldots)^2 \\
&\quad - a\varepsilon^{\mu+\frac{3}{2}} + a\varepsilon^{2\mu}(u_0 + \varepsilon u_1(\xi) + \ldots) \\
&\quad - \varepsilon^{\mu+\frac{1}{2}}(p_0 + \varepsilon p_1(\xi) + \ldots)(c + s\varepsilon^{\mu+\frac{3}{2}}), && (3.13)\\
\dot{v}_0(\xi) + \varepsilon\dot{v}_1(\xi) + \varepsilon^2\dot{v}_2(\xi) + \ldots &= q_0(\xi) + \varepsilon q_1(\xi) + \varepsilon^2 q_2(\xi) + \ldots, && (3.14)\\
\dot{q}_0(\xi) + \varepsilon\dot{q}_1(\xi) + \ldots &= am(v_0(\xi) + \varepsilon v_1(\xi) + \ldots) \\
&\quad - (u_0 + \varepsilon u_1(\xi) + \ldots)(v_0(\xi) + \varepsilon v_1(\xi) + \ldots)^2 \\
&\quad - s\varepsilon^2(q_0(\xi) + \varepsilon q_1(\xi) + \ldots). && (3.15)
\end{aligned}$$

From equation (3.13) we find:

$$\dot{p}_1(\xi) = u_0 v_0^2,$$

by collecting terms of $\mathcal{O}(\varepsilon)$. This leads to:

$$p_1(\xi) = \int_0^\xi u_0 v_0^2(\tau)d\tau + p_1(0).$$

Because u_0 is a constant and v_0 is known (the homoclinic solution of the unperturbed system), $p_1(\xi)$ can be determined explicitly:

$$\begin{aligned}
p_1(\xi) - p_1(0) &= u_0 \int_0^\xi v_0^2(\tau)d\tau \\
&= u_0 \int_0^\xi \left(\frac{3b}{2u_0}\right)^2 \operatorname{sech}^4\left(\frac{\sqrt{b}}{2}\tau\right) d\tau \\
&= \frac{9b^2}{4u_0} \int_0^\xi \operatorname{sech}^4\left(\frac{\sqrt{b}}{2}\tau\right) d\tau \\
&= \frac{3b\sqrt{b}}{2u_0} \tanh\left(\frac{\sqrt{b}\xi}{2}\right)\left(\operatorname{sech}^2\left(\frac{\sqrt{b}}{2}\xi\right) + 2\right)
\end{aligned}$$

Note that $\operatorname{sech}^2(\xi)$ is an even function, and $\tanh(\xi)$ is odd, hence p_1 is an odd function.

In a similar way, we obtain from (3.12):

$$\dot{u}_1 = p_0.$$

From this, since p_0 is constant, elementary calculus gives a solution $u_1(t) = u_{1,0} + p_0 t$, with $u_{1,0}$ some unknown constant. It is natural to assume the solutions of interest to be bounded. This is not the case if $u_1(t)$ is not bounded, hence, this leads to $p_0 = 0$. Moreover, as the initial condition we assumed that $u_j(0) = 0$ for all $j \geq 1$. This yields that $u_{1,0} = 0$ and hence $u_1(t) \equiv 0$.

Now, consider ΔK

$$\begin{aligned}\Delta K &= \int_{-\frac{1}{\sqrt{\varepsilon}}}^{\frac{1}{\sqrt{\varepsilon}}} \dot{K} d\xi, \\ &= \int_{-\frac{1}{\sqrt{\varepsilon}}}^{\frac{1}{\sqrt{\varepsilon}}} \frac{1}{3}\varepsilon p v^3 - s\varepsilon^2 q^2 d\xi, \\ &= \int_{-\frac{1}{\sqrt{\varepsilon}}}^{\frac{1}{\sqrt{\varepsilon}}} \frac{1}{3}\varepsilon(p_0 + \varepsilon p_1 + \ldots)(v_0 + \varepsilon v_1 + \ldots)^3 - s\varepsilon^2(q_0 + \varepsilon q_1 + \ldots)^2 d\xi,\end{aligned}$$

where p_1, v_0, v_1, q_0 and q_1 still depend on ξ.
From this it follows that a first condition for $\Delta K = 0$ is that $p_0 = 0$ because that term can never be balanced. Next, collecting terms yields:

$$\Delta K = \varepsilon^2 \int_{-\frac{1}{\sqrt{\varepsilon}}}^{\frac{1}{\sqrt{\varepsilon}}} \frac{1}{3} p_1(\xi) v_0^3(\xi) - s q_0^2(\xi) d\xi + \mathcal{O}(\varepsilon^2). \tag{3.16}$$

Now substituting the expressions we already obtained for v_0, p_1 and q_0 into (3.16) and integrating, yields the following expression for ΔK

$$\Delta K = \frac{6\varepsilon^2 b^2 \sqrt{b}}{5u_0^2}\left[\frac{2p_1(0)}{u_0} - s\right] + \mathcal{O}(\varepsilon^3). \tag{3.17}$$

The derivation of this expression depends highly on the odd/even characteristics of v_0 and p_1, because many terms cancel when integrating over a symmetric domain. Recall that this ΔK was used as a distance measurement of $W^s(\mathcal{M})$ and $W^u(\mathcal{M})$. In the construction of a homoclinic orbit we need $\Delta K = 0$. A first order requirement for this is that at least at the $\mathcal{O}(\varepsilon^2)$ level, $\Delta K = 0$. This leads to:

$$p_1(0) = \frac{1}{2} s u_0$$

Now note that $p_1(0)$ and u_0 are constants. This means that for every pair u, p for which

$$p = \frac{1}{2} s u \tag{3.18}$$

holds, ΔK has zeros. Thus, this relation between p and u yields a leading order description of $W^s(\mathcal{M}) \cap W^u(\mathcal{M})$ on the $\mathcal{O}(\varepsilon^2)$ level. Higher order terms cannot perturb this result in such a way that there does not exist an intersection. This means that there are indeed orbits homoclinic to the manifold $\mathcal{M}$ if p and u are related according to (3.18).

3.4 Take off and Touch down curves

In the previous section, a condition was derived for intersections of the stable and unstable manifolds of $\mathcal{M}$. In this section, the relationship between the slow and the fast dynamics in (2.4) will be elaborated. The so-called take-off and touch-down curves will be computed. These are the sets of base points associated to sets of orbits in $W^u(\mathcal{M})$ and $W^s(\mathcal{M})$ respectively.

3.4.1 Fenichel theory

For this section, first some preliminaries about Fenichel theory are necessary. The definition and theorems that follow are adopted from [6]. The theory that is needed

for the derivation of the take-off and touch-down curves that will be defined in this section revolves around Fenichel's third theorem, which deals with Fenichel fibers and base points. First, a notation is introduced: $x \cdot t$ is used to denote the application of a flow after time t to an initial point x. This notation can be extended such that $V \cdot t$, where V is a set, is the application of a flow after time t to the entire set, and $x \cdot [t_1, t_2]$ is the trajectory that is the result when the flow is applied over the interval $[t_1, t_2]$. The set Δ will be defined as a neighborhood of $\mathcal{M}$ to avoid difficulties [6].

Definition 1. The *forward evolution* of a set $V \subset \Delta$, restricted to Δ is given by the set:

$$V \cdot_\Delta t := \{x \cdot t : x \in V \text{ and } x \cdot [0, t] \subset \Delta\}.$$

This is needed for the following theorem, known as Fenichel's third theorem.

Theorem 3 (Fenichel's third theorem)**.** *Suppose $\mathcal{M}_0 \subset \{q = 0, bv - uv^2 - s\varepsilon^2 q = 0\}$ is compact, possibly with boundary, and normally hyperbolic. Suppose the equations describing the flow are smooth. Then for every $v_\varepsilon \in \mathcal{M}_\varepsilon$, $\varepsilon > 0$ and sufficiently small, there are one-dimensional manifolds $W^s(v_\varepsilon) \subset W^s(\mathcal{M}_\varepsilon)$ and $W^s(v_\varepsilon) \subset W^s(\mathcal{M}_\varepsilon)$ that are $\mathcal{O}(\varepsilon)$ close and diffeomorphic to $W^s(v_0)$ and $W^u(v_0)$, where v_0 is the counterpart of v_ε in the unperturbed setting. The families $\{W^{u,s}(v_\varepsilon) : v_\varepsilon \in \mathcal{M}_\varepsilon\}$ are invariant in the sense that*

$$W^s(v_\varepsilon) \cdot_\Delta \xi \subset W^s(v_\varepsilon \cdot \xi)$$

if $v_\varepsilon \cdot s \in \Delta$ for all $s \in [0, \xi]$ and

$$W^u(v_\varepsilon) \cdot_\Delta \xi \subset W^u(v_\varepsilon \cdot \xi)$$

if $v_\varepsilon \cdot s \in \Delta$ for all $s \in [\xi, 0]$.

This theorem seems a bit indistinct at first, but for this thesis it will not be too important. Mostly it was included here for completeness with respect to Fenichel's first and second theorem and to use the corollary that is stated below. This corollary can also be found in [6]. The Fenichel fibers, see [6], give a correspondance between points in $W^{s,u}(\mathcal{M}_\varepsilon)$ and $\mathcal{M}_\varepsilon$. A point $w \in W^s(\mathcal{M}_\varepsilon)$ has an associated *base point* $w^+ \in \mathcal{M}_\varepsilon$ such that $w \in W^s(w^+)$. Analogously, a point $w \in W^u(\mathcal{M}_\varepsilon)$ has a base point $w^- \in M_\varepsilon$ such that $w \in W^u(w^-)$.

Corollary 1. *There exist constants $\kappa_s, \alpha_s > 0$ such that if $w \in W^s(w^+) \cap \Delta$, then*

$$||w \cdot \xi - w^+ \cdot \xi|| \leq \kappa_s e^{-\alpha_s \xi}$$

for all $\xi \geq 0$ for which $w \cdot [0, \xi] \subset \Delta$ and $w^+ \cdot [0, \xi] \subset \Delta$.
Similarly, there are constants $\kappa_u, \alpha_u > 0$ such that if $w \in W^u(w^-) \cap \Delta$, then

$$||w \cdot \xi - w^- \cdot \xi|| \leq \kappa_u e^{\alpha_u \xi}$$

for all $\xi \leq 0$ for which $w \cdot [\xi, 0] \subset \Delta$ and $w^- \cdot [\xi, 0] \subset \Delta$.

These estimates yield that if a point $w \in W^s(\mathcal{M}_\varepsilon)$ has base point $w^+ \in \mathcal{M}_\varepsilon$, there are constants C_1, C_2, κ such that

$$||w \cdot T - w^+ \cdot T|| \leq C_1 e^{-\kappa/\varepsilon} \quad \forall T \geq \frac{C_2}{\varepsilon},$$

and analogous for $W^u(\mathcal{M}_\varepsilon)$. The take-off and touch-down curves are in fact sets of base points associated to sets of orbits in $W^{s,u}(\mathcal{M})$.

The first intersection point of the stable and unstable manifold with the hyperplane $\{q = 0\}$ is described by (3.18). This describes a one-dimensional curve in $W^s(\mathcal{M}) \cap W^u(\mathcal{M})$. Through any point, w, on this curve, there is an orbit $\Gamma(\xi; w)$ which approaches $\mathcal{M}$ for both large positive and negative ξ. This is because the curve is a subset of both the stable and unstable manifold of $\mathcal{M}$. To be more exact, Fenichel's third theorem (above), implies that for any such $\Gamma(\xi, w)$ there exist two orbits $\Gamma^+_{\mathcal{M}}(\xi; w^+)$ and $\Gamma^-_{\mathcal{M}}(\xi; w^-)$, both subsets of $\mathcal{M}$ where $\Gamma^\pm_{\mathcal{M}}(0; w^\pm) = w^\pm \in \mathcal{M}$. For these orbits, the corollary gives us that

$$\| \Gamma(\xi; w) - \Gamma^+_{\mathcal{M}}(\xi; w^+) \|,$$

is exponentially small for $\xi > 0$ and $\xi = \mathcal{O}(\frac{1}{\varepsilon})$. The same holds for $\Gamma^-_{\mathcal{M}}(\xi; x^-)$ and $\xi < 0$ and $|\xi| \geq \mathcal{O}(\frac{1}{\varepsilon})$. As a consequence, $\Gamma(\xi, w)$ must lie exponentially close to $\mathcal{M}$ during the slow parts of the orbit, and $\Gamma^\pm_{\mathcal{M}}(\xi; w^\pm)$ determine the behavior of $\Gamma(\xi, w)$.
Now note that for $\xi = 0$ we have $\Gamma^\pm_{\mathcal{M}}(0; w^\pm) = w^\pm \in \mathcal{M}$, and these base points $w^\pm$ form the take off and touch down curves.

$$T_o = \bigcup_w \left\{ w^- = \Gamma^-_{\mathcal{M}}(0; w^-) \right\},$$
$$T_d = \bigcup_w \left\{ w^+ = \Gamma^+_{\mathcal{M}}(0; w^+) \right\}.$$

Here, the unions are over all $w \in W^s(\mathcal{M}) \cap W^u(\mathcal{M}) \cap \{q = 0\}$. The take-off set T_o represents all base points of Fenichel fibers in $W^u(\mathcal{M})$ that are asymptotic to $\mathcal{M}$ as $\xi \to \infty$. Analogously, the touch-down set T_d represents all base points of Fenichel fibers in $W^s(\mathcal{M})$ which are asymptotic to $\mathcal{M}$ as $\xi \to -\infty$.

3.4.2 QUANTIFICATION

In this section the take-off and touch-down sets will be determined explicitly as relations between p and u. It will be determined with methods similar to [2], [3], [6]. The underlying thought in the derivatoin is that the change of p is measured during half a circuit through the fast field, because $\xi = 0$ at the base point. This accumulated change can be measured by integrating $\dot{p}$ along the orbit until it settles down near $\mathcal{M}$. Again, the interval I_f will be used to integrate the leading order change of p during the fast circuit. The change of p during the fast circuit can be measured as:

$$\begin{aligned}
\Delta p &= \int_{I_f} \dot{p} d\xi, \\
&= \varepsilon \int_{-\frac{1}{\sqrt{\varepsilon}}}^{\frac{1}{\sqrt{\varepsilon}}} (u(\xi)v^2(\xi) + \mathcal{O}(\varepsilon^2)) d\xi, \\
&= \varepsilon \int_{-\frac{1}{\sqrt{\varepsilon}}}^{\frac{1}{\sqrt{\varepsilon}}} u_0 v_0^2(\xi) d\xi + \mathcal{O}(\varepsilon^2), \\
&= \varepsilon \frac{6b\sqrt{b}}{u_0} + \mathcal{O}(\varepsilon^2),
\end{aligned}$$

The same integral was computed in section 3.3, here the limits were only adjusted. And from here, the change in u can be computed.

$$\Delta u = \int_{I_f} \dot{u} dt = \int_{I_f} \varepsilon p dt,$$

so $\Delta u = \mathcal{O}(\varepsilon^2)$ because $p = \mathcal{O}(\varepsilon)$. This also relates to the pulses, see figures 2.1 and 2.2, where we see that during the fast excursion the value of u does not change so much, but the sign of p changes so the change in p is larger than the change in u.

As stated above, homoclinic solutions consist of two parts close to the manifold $\mathcal{M}$, and one fast excursion through the fast field. Now, it is clear where the transitions between these parts are; this is namely captured by the take-off and touch-down curves.

An explicit expression for T_o and T_d can be obtained by determining the relation between the base points $w^{\pm}$ and the point w. The integration above was during a full circuit through the fast field. However, just half of this excursion determines the relation between one of the base points and the point w, these are given by

$$\int_{-\frac{1}{\sqrt{\varepsilon}}}^{0} \dot{p} d\xi \qquad \text{and} \qquad \int_{0}^{\frac{1}{\sqrt{\varepsilon}}} \dot{p} d\xi$$

for $t < 0$ and $t > 0$ respectively. Since to leading order, $\dot{p} = \varepsilon u_0 v_0^2(\xi)$, and v_0 is an even function, it is easily verified that

$$\int_{-\frac{1}{\sqrt{\varepsilon}}}^{0} \dot{p} d\xi = \int_{0}^{\frac{1}{\sqrt{\varepsilon}}} \dot{p} d\xi = \frac{1}{2} \int_{-\frac{1}{\sqrt{\varepsilon}}}^{\frac{1}{\sqrt{\varepsilon}}} \dot{p} d\xi,$$

which was computed above. So:

$$\int_{-\frac{1}{\sqrt{\varepsilon}}}^{0} \dot{p} d\xi = \int_{0}^{\frac{1}{\sqrt{\varepsilon}}} \dot{p} d\xi = \varepsilon \frac{3b\sqrt{b}}{u_0}.$$

Since w must also satisfy (3.18) the symmetry property yields two sets of base points. The take-off and touch-down curves are to leading order:

$$T_o : \qquad p = \frac{1}{2}\varepsilon \left(su - \frac{6b\sqrt{b}}{u} \right), \tag{3.19}$$

$$T_d : \qquad p = \frac{1}{2}\varepsilon \left(su + \frac{6b\sqrt{b}}{u} \right). \tag{3.20}$$

This means that the take-off and touch-down sets are in fact curves in $\mathcal{M}$. They are depicted in figure 3.2. Again, note we zoomed into the horizontal axis. The take-off and touch-down curves are of the same magnitude as $\ell^{s,u}$, namely $\mathcal{O}(\varepsilon)$. The take-off and touch-down curves will be of crucial importance in the construction of homoclinic and periodic orbits.

Chapter 4

A homoclinic orbit

A natural question that arises when constructing periodic solutions, is whether or not homoclinic solutions can exist. Often these solutions are easier to construct explicitly and they can be regarded as periodic solutions with an infinite period. In this chapter, a condition for the existence of homoclinic and periodic orbits will be derived. Under that condition, a geometric proof for existence of homoclinic orbits will be given.

4.1 Condition

Homoclinic solutions follow the unstable manifold ℓ^u of P, then jump through the fast field at the point of intersection with T_o with a certain u-coordinate, $\tilde{u}$. And, they return to $\mathcal{M}$ at the point on T_d with u-coordinate $\tilde{u}$. For a homoclinic orbit, this return point should also intersect with the stable manifold ℓ^s of P, in order to arrive at P for $\xi \to \infty$. A priori, this might not be possible. To illustrate the possibilities, see the figures in 4.1.

For a situation in the right figure of 4.1, solutions will touch down to the right-hand side of the stable manifold ℓ^s. These solutions grow unboundedly and will never return to ℓ^s. An intersection of T_d and ℓ^s is necessary for the existence of a homoclinic orbit. This means that, in figure 4.1, the right figure cannot yield any homoclinic, or even periodic solutions. The distinction between the two figures in figure 4.1 depends on the parameter c, i.e. the slope of the terrain, with respect to s, the wave speed.
One can immediately expect that there must exist a transition point, where ℓ^s and T_d are tangent. This is depicted in figure 4.2. This transition point can be determined explicitly.

For a intersection point of ℓ^s and T_d it holds that:

$$p = \frac{1}{2}\varepsilon\left(su + \frac{6b\sqrt{b}}{u}\right) \qquad \text{Touch-down} \tag{4.1}$$

$$p = \frac{1}{2}\varepsilon\left(c + \sqrt{c^2+4a}\right) \qquad \ell^s \tag{4.2}$$

Equating these, one finds:

$$su + \frac{6b\sqrt{b}}{u} = c + \sqrt{c^2+4a} \quad \Rightarrow \quad su^2 - cu - \sqrt{c^2+4a} + 6b\sqrt{b} = 0,$$

which is a quadratic polynomial in u. The tangency of ℓ^s with T_d is equivalent to them having exactly one intersection point. This holds when the discriminant of the quadratic polynomial is zero. In a more explicit way, the tangency holds when:

$$(-c - \sqrt{c^2+4a})^2 - 24sb\sqrt{b} = 0.$$

And from here it is easily determined that the transition point lies at

$$s = \frac{(c + \sqrt{c^2+4a})^2}{24b\sqrt{b}}. \tag{4.3}$$

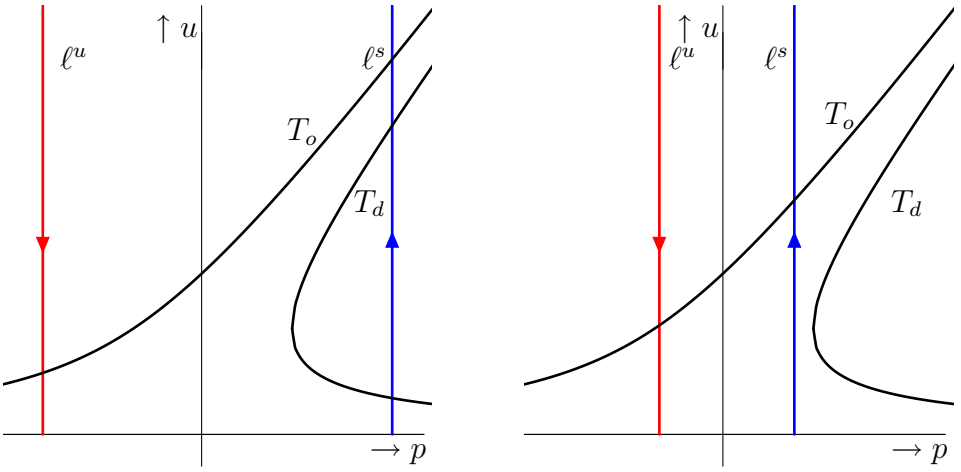

Figure 4.1: Schematic pictures of the take-off and touch-down curves on $\mathcal{M}$ together with the stable and unstable manifold $\ell^{s,u}$ of P. On the left, the T_d and ℓ^s intersect, on the right, they do not. This is related to the magnitude of c compared to s. On the left, $s < \frac{(-c-\sqrt{c^2+4a})^2}{24b\sqrt{b}}$, on the right, $s > \frac{(-c-\sqrt{c^2+4a})^2}{24b\sqrt{b}}$.

Moreover, from here it can be determined that T_d and ℓ^s intersect if and only if:

$$s \leq \frac{(-c-\sqrt{c^2+4a})^2}{24b\sqrt{b}}. \tag{4.4}$$

So this is a condition for the existence of both homoclinic and periodic orbits. Moreover, it is realistic to require s to be positive because this is the direction of the traveling pattern. A positive s value corresponds to the direction uphill, which was the behavior that was described in [7].
The speed of the pulse is allowed to take values in the range:

$$0 \leq s \leq \frac{(-c-\sqrt{c^2+4a})^2}{24b\sqrt{b}}. \tag{4.5}$$

This means that if $c \to \infty$, the possible values for s will be in a larger range, but as c becomes small, the traveling pulse will tend to be stationary. This is the case which was discussed in [3].

4.2 Existence

In this section, the existence of a homoclinic orbit will be proved. In doing so, a value s^* for which the u-coordinate of $T_o \cap \ell^u$ and $T_d \cap \ell^s$ are equal needs to be determined. It can be shown that indeed, a homoclinic orbit exist for all $a, b, c > 0$. This is formulated in the following theorem.

Theorem 4. *For every $a, b, c > 0$ there exists an ε_0 such that for all $\varepsilon < \varepsilon_0$ there exists a unique s^* for which the system (2.4), possesses a fast-slow orbit homoclinic to P, i.e. that system (1.4) has a traveling pulse solution with speed s^*. This s^* is given by:*

$$s^* = \frac{s\sqrt{c^2+4a}}{6b\sqrt{b}}$$

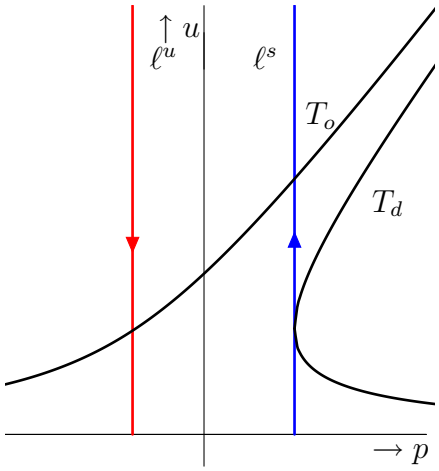

Figure 4.2: Sketch of the take-off and touch-down curves on $\mathcal{M}$ together with the stable and unstable manifold $\ell^{s,u}$ of P. Here, the tangent point of ℓ^s and T_d is depicted, where $s = \frac{(-c-\sqrt{c^2+4a})^2}{24b\sqrt{b}}$.

Proof. This proof will consist of two steps. First the existence of the homoclinic orbit will be proved by showing that there exists an s^* such that $W^u(P)$ and $W^s(P)$ have a one-dimensional intersection (i.e. the orbit itself, parametrized by ξ). The second step will be the quantification of s^* and the verification that it satisfies condition (4.5).

Recall that $W^{s,u}(P)$ are two-dimensional manifolds, $W^{s,u}(\mathcal{M})$ are three- dimensional manifolds, and $\mathcal{M}$ is a two-dimensional manifold in $\mathbb{R}^4$. In the first step, it will be assumed that s is such that it satisfies (4.5), this will be verified in the second part of the proof.

Generically, two two-dimensional manifolds have a zero-dimensional intersection in $\mathbb{R}^4$. This indicates that not for every s there exists a homoclinic orbit. For this there needs to be a certain s^* such that this intersection is one-dimensional, i.e. the orbit Γ.
For a given traveling wave speed s there are two generic options for the position of the take-off and touch-down curves with respect to $\ell^{s,u}$ on $\mathcal{M}$. The explicit expressions for these curves are given in (3.4), (3.19) and (3.20). The two generic cases are depicted in figure 4.3. It follows from the analysis in chapter 3 that $\ell^{s,u}$ are one-dimensional and to leading order parallel to the u-axis, and not symmetric around the u-axis. The pictures are thus not to scale! This figure is merely to sketch the geometry of the structure on $\mathcal{M}$ and to show that the stable and unstable manifold are indeed attached to the equilibrium P.

The take-off and touch-down curves were constructed such that they represent all points on $\mathcal{M}$ that leave $\mathcal{M}$ *and* return to it, i.e. all points such that the corresponding jump through the fast field is homoclinic to $\mathcal{M}$. In the construction it was assumed that u is constant during this fast excursion. A homoclinic orbit to P must, by definition, leave P in the direction of ℓ^u. It will take-off for a fast excursion when the orbit gets near the take-off curve, and during this excursion the u-coordinate is constant to leading order, $u = \tilde{u}$, which is also depicted in Figure 4.3. Because of this construction, it is determined where the orbit will touch-down on (actually exponentially close to) $\mathcal{M}$ again. From Figure 4.3 it is clear that for a homoclinic connection, the touch-down point of the homoclinic orbit should be

exactly on ℓ^s.

Define u_P to be the u-coordinate of the fixed point P, $u_P = \frac{\varepsilon\sqrt{\varepsilon}}{\delta}$. Now introduce any $tilde u < \bar{u} < u_P$, recall that $\tilde{u}$ is the u-coordinate of the take-off point. Consider the intersection of $\{u = \bar{u}\}$ with $W^s(\mathcal{M})$, both three-dimensional subsets of $\mathbb{R}^4$. Generically these have a two-dimensional intersection. This will be verified here. The hyperplane $\{u = \bar{u}\}$ divides $\mathbb{R}^4$ into two distinct parts, like a line divides the plane. In the case that $\varepsilon = 0$, $W^s(\mathcal{M}_0) \not\subset \{u = \bar{u}\}$, which means that the intersection cannot be three-dimensional.

Restricted to $\mathcal{M}_0$, for $\varepsilon = 0$, the intersection $\{u = \bar{u}\} \cap W^s(\mathcal{M}_0)$ is transversal. Moreover, $\mathcal{M}_0$ has a transversal intersection with $\{u = \bar{u}\}$ itself and hence $\{u = \bar{u}\} \cap W^s(\mathcal{M}_0)$ is transversal in $\mathbb{R}^4$. If this holds for $\mathcal{M}_0$, then the first and second theorem of Fenichel yields that it is true for $\mathcal{M}_\varepsilon = \mathcal{M}$ as well. This means $\{u = \bar{u}\} \cap W^s(\mathcal{M})$ is two-dimensional. This intersection is represented by the pink area in figure 4.4.

For $W^s(P)$, which is a subset of $W^s(\mathcal{M})$ because $P \in \mathcal{M}$, the same reasoning holds, so $W^s(P) \cap \{u = \bar{u}\}$ is one-dimensional, depicted in blue in figure 4.4.
Moreover, $\mathcal{M} \cap \{u = \bar{u}\}$ is one-dimensional, and parallel to the p-axis. This follows from the definition of $\mathcal{M}$. And this also means that $(\mathcal{M} \cap W^s(P)) \cap \{u = \bar{u}\}$ intersect in a zero-dimensional subspace, i.e. a point.

The gray orbit in figure 4.3 represents an orbit $\gamma(\xi)$ with the property that $\lim_{\xi \to -\infty} \gamma_\xi = P$. It is an orbit $\gamma(\xi) \in W^u(P) \cap W^s(\mathcal{M})$. It is one-dimensional and since it takes off and touches down on $\mathcal{M}$ again, it must be in the stable manifold of $\mathcal{M}$. Moreover, it is a one-dimensional set, so intersection with the three-dimensional $\{u = \bar{u}\}$ yields a zero-dimensional set. Also, because $\bar{u} > \tilde{u}$, the orbit has flowed past the touched down point and is exponentially close to $\mathcal{M}$ already. From the geometry of the take-off and touch-down curves in figure 4.3 it follows that $\gamma(\xi) \cap \{u = \bar{u}\}$ lies either on the left-hand or on the right-hand side of $W^s(P) \cap \{u = \bar{u}\}$. This explains the black dots in 4.4, which is the intersection of the orbit with $\{u = \bar{u}\}$. Combining all these verifications the intersection of $\{u = \bar{u}\}$ with the phase space results in figure 4.4.

Because of continuity, there must be a unique s^* such that the touch-down point is exactly on $W^s(P)$. This corresponds to figure 4.5. In this case, the intersection $W^s(P) \cap W^u(P)$ is one-dimensional, and a unique homoclinic orbit exists.

The expression for s^* can be determined explicitly, because there are explicit expressions for $\ell^{s,u}$ and T_o and T_d. This will be the second step of the proof. Two conditions must be satisfied for $\tilde{u}$ and a given c:

$$\begin{aligned} T_o \cap \ell^u : c - \sqrt{c^2 + 4a} &= su - 6\frac{b\sqrt{b}}{u} \\ T_d \cap \ell^s : c + \sqrt{c^2 + 4a} &= su + 6\frac{b\sqrt{b}}{u}, \end{aligned} \tag{4.6}$$

which are just the expressions that were obtained in Chapter 3.
This implies that:

$$s^*\tilde{u} = c,$$

and

$$\sqrt{c^2 + 4a} = 6\frac{b\sqrt{b}}{\tilde{u}},$$

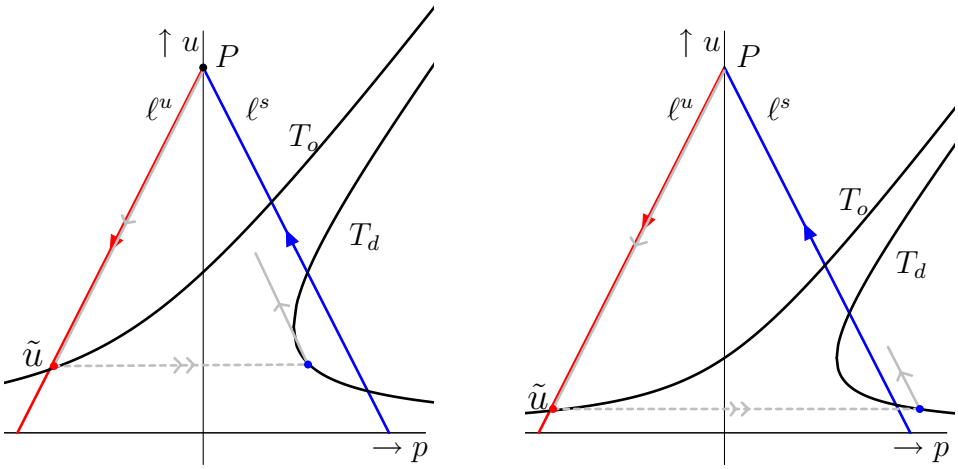

Figure 4.3: Schematic pictures of the take-off and touch-down curves on $\mathcal{M}$ with $s > s^*$ (left) and $s < s^*$ (right). In red $W^u(P) \cap \mathcal{M}$, in blue $W^s(P) \cap \mathcal{M}$. The gray line displays an orbit starting on the unstable manifold of P with a fast excursion denoted by the dashed line. The stable and unstable manifold restricted to $\mathcal{M}$ are not to scale with the take-off and touch-down curves, see Figure 3.2.

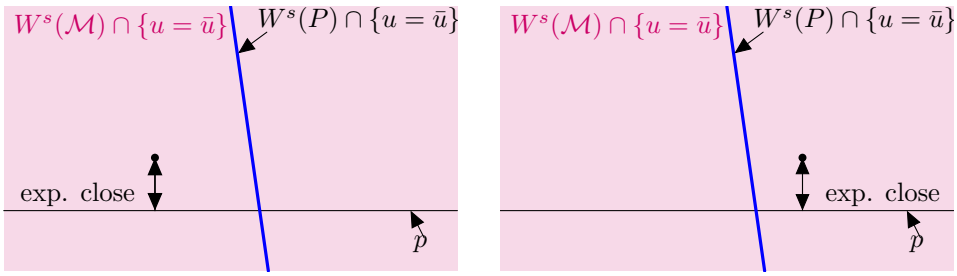

Figure 4.4: Intersection of $W^s(\mathcal{M})$ with $\{u = \bar{u}\}$ where the horizontal coordinate is p. The blue line is $W^s(P) \cap \{u = \bar{u}\}$, the black dots the orbits that took off at the intersection point of ℓ^u with T_o and has touched down already, displayed as intersection with $\{u = \bar{u}\}$. On the left, the case where $s > s^*$ and on the right, the case where $s < s^*$. The intersection of $\mathcal{M}$ with $\{u = \bar{u}\}$ is parallel to the p-axis on $\mathcal{M}$. The horizontal coordinate is therefore p.

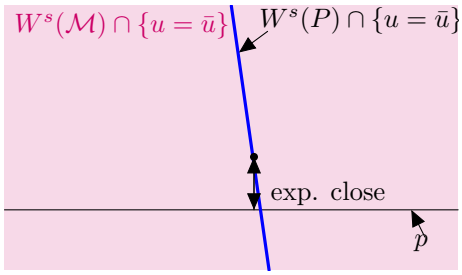

Figure 4.5: The homoclinic solution depicted in $W^s(\mathcal{M}) \cap \{u = \bar{u}\}$ where the horizontal coordinate is p. The blue line is $W^s(P) \cap \{u = \bar{u}\}$, the black dot the orbits that took off at the intersection point of ℓ^u with T_o and has touched down already, displayed as intersection with $\{u = \bar{u}\}$. In this figure $s = s^*$.

and hence:

$$s^* = \frac{c\sqrt{c^2 + 4a}}{6b\sqrt{b}}, \tag{4.7}$$

$$\tilde{u} = \frac{6b\sqrt{b}}{\sqrt{c^2 + 4a}}. \tag{4.8}$$

Next, it needs to be verified for which c, condition (4.5) is satisfied. Thus, we need that:

$$s^* \leq \frac{(c + \sqrt{c^2 + 4a})^2}{24b\sqrt{b}}.$$

We find

$$\begin{aligned}
\frac{c\sqrt{c^2 + 4a}}{6b\sqrt{b}} &\leq \frac{(c + \sqrt{c^2 + 4a})^2}{24b\sqrt{b}} \\
4c\sqrt{c^2 + 4a} &\leq (c + \sqrt{c^2 + 4a})^2 \\
4c\sqrt{c^2 + 4a} &\leq c^2 + 2c\sqrt{c^2 + 4a} + c^2 + 4a \\
0 &\leq c^2 - 2c\sqrt{c^2 + 4a} + c^2 + 4a \\
0 &\leq (c - \sqrt{c^2 + 4a})^2.
\end{aligned}$$

And since the latter states that a real-valued square is larger than zero, which is obviously the case for all c. Also, as $a, b, c > 0$ the condition that $s^* > 0$ is also satisfied.

From here we can conclude that for $s = s^*$, there exists a homoclinic orbit, for any c. Of course, this analysis was based on approximations of T_d and T_o and $\ell^{s,u}$, which were based on expansions in ε. This means that the analysis only holds for ε small enough, such that these approximations remain valid. □

So a homoclinic solution exists for every c. Such a pulse corresponds to a single traveling vegetation strip in an endless sloped desert: a traveling oasis on a hill. However, we do not claim that the model (1.4) is really suitable to describe this kind of behavior. For example, an actual water source cannot be modeled by (1.4).

Again, note that we need $s > 0$ as well, because this corresponds to the vegetation traveling in the opposite direction (uphill) of the water flow (downhill), which was observed and described in [7].

We now have for the homoclinic solution that

$$s^* = \frac{c\sqrt{c^2+4a}}{6b\sqrt{b}}$$

and the corresponding u-value during the fast circuit

$$\tilde{u} = \frac{6b\sqrt{b}}{\sqrt{c^2+4a}}.$$

For a very 'flat' hill, i.e. $0 < c \ll 1$, this yields:

$$s = \frac{c\sqrt{a}}{3b\sqrt{b}} + h.o.t.$$

which tends to zero as $c \to 0$. This means that the flatter the hill, the slower the homoclinic pulse moves upwards. This corresponds to [3], where stationary homoclinic pulses were constructed for $c = 0$, and $u = \frac{3b\sqrt{b}}{\sqrt{a}}$, which corresponds to our expression.
For a very steep hill, $c \gg 1$ it follows that

$$s = \frac{c^2}{6b\sqrt{b}} + h.o.t.$$

which determines that $s \to \infty$ as $c \to \infty$. So a steeper hill results in a faster traveling speed of the homoclinic pulse.

Chapter 5

Periodic orbits

A natural question that arises when the homoclinic pulse is constructed, is whether or not this construction can be pursued for periodic solutions. In [3], this question is addressed by parameterizing the orbits on $\mathcal{M}$ and performing a similar analysis to Chapter 4. In [3], the result is that the periodic orbits exist only for a specific range of parameter values. The system exhibits a saddle-node bifurcation where pairs of periodic orbits collide and disappear. On the other hand, as the period goes to infinity, the periodic orbits become homoclinic orbits. This presents a range of parameter values for which periodic orbits exist.

One could expect this result to be the case for (2.4) as well. Our first attempt to prove such an existence theorem is to construct periodic orbits in (2.4) and apply the methods used in [3]. Therefore, we aim to find a parametrization of the orbits on $\mathcal{M}$. First, note that periodic orbits must be bounded in particular. All orbits on $\mathcal{M}$ that lie outside of the area enclosed by $\ell^{s,u}$ are not. This follows from the structure of the slow subsystem (3.1). We must restrict to the bounded area enclosed by $\ell^{s,u}$. For notational purposes it is therefore useful to introduce:

$$\mathcal{A} := \left\{ (u,p) \in \left(-\infty, \varepsilon^{\frac{3}{2}-\mu}\right] \times \left[\frac{1}{2}\varepsilon\left(c - \sqrt{c^2+4a}\right), \frac{1}{2}\varepsilon\left(c + \sqrt{c^2+4a}\right)\right] \right\} \tag{5.1}$$

which is the area of interest on $\mathcal{M}$ for this chapter. The area $\mathcal{A}$ represents that part of $\mathcal{M}$ which is enclosed by the stable and unstable manifold of P. Note that this makes $\mathcal{A}$ invariant because $\ell^{s,u}$ are orbits in particular.

5.1 Direct calculation

The behavior on $\mathcal{M}$ is described by:

$$\begin{aligned} u_\xi &= \varepsilon p, \\ p_\xi &= \varepsilon\left[-a\sqrt{\varepsilon}\delta\left(1 - \frac{\delta}{\varepsilon\sqrt{\varepsilon}}u\right)\right] - \sqrt{\varepsilon}\delta p\left(c + s\varepsilon\sqrt{\varepsilon}\delta\right), \end{aligned} \tag{5.2}$$

or, in matrix representation

$$\begin{pmatrix} u_\xi \\ p_\xi \end{pmatrix} = \begin{pmatrix} 0 & \varepsilon \\ a\delta^2 & -\sqrt{\varepsilon}\delta(c + s\varepsilon\sqrt{\varepsilon}\delta) \end{pmatrix}\begin{pmatrix} u \\ p \end{pmatrix} + \begin{pmatrix} 0 \\ -a\varepsilon\sqrt{\varepsilon}\delta \end{pmatrix} \tag{5.3}$$

The problem here is that this is not a small perturbation of a Hamiltonian system, a nearly integrable system, and hence the orbits on $\mathcal{M}$ cannot be described conveniently as level sets, such as in [3]. We will use a rescaling to modify the system into a nearly integrable system. First scale $x = u - \frac{\varepsilon\sqrt{\varepsilon}}{\delta}$ and $y = p$ to shift the fixed point to the origin. We obtain:

$$\begin{pmatrix} x_\xi \\ y_\xi \end{pmatrix} = \begin{pmatrix} 0 & \varepsilon \\ a\delta^2 & -\sqrt{\varepsilon}\delta(c + s\varepsilon\sqrt{\varepsilon}\delta) \end{pmatrix}\begin{pmatrix} x \\ y \end{pmatrix}. \tag{5.4}$$

Next, the matrix

$$\begin{pmatrix} 0 & \varepsilon \\ a\delta^2 & -\sqrt{\varepsilon}\delta(c + s\varepsilon\sqrt{\varepsilon}\delta) \end{pmatrix}$$

can be diagonalized, by a transformation T, which is composed of the eigenvectors:

$$T = \begin{pmatrix} \frac{\varepsilon}{\lambda_+} & \frac{\varepsilon}{\lambda_-} \\ 1 & 1 \end{pmatrix},$$

with eigenvalues

$$\lambda_\pm = \frac{1}{2}\left[-\sqrt{\varepsilon}\delta(c + s\varepsilon\sqrt{\varepsilon}\delta) \pm \sqrt{(-\sqrt{\varepsilon}\delta(c + s\varepsilon\sqrt{\varepsilon}\delta))^2 + 4a\varepsilon\delta^2}\right].$$

Hence, we introduce

$$\begin{pmatrix} \tilde{x} \\ \tilde{y} \end{pmatrix} = T \begin{pmatrix} x \\ y \end{pmatrix}.$$

Then the system (5.2) becomes:

$$\begin{pmatrix} \tilde{x}_\xi \\ \tilde{y}_\xi \end{pmatrix} = \begin{pmatrix} \lambda_+ & 0 \\ 0 & \lambda_- \end{pmatrix} \begin{pmatrix} \tilde{x} \\ \tilde{y} \end{pmatrix}. \tag{5.5}$$

This is still not a Hamiltonian system, but the solutions can be described as level sets in $\mathcal{M}$, by means of solving (5.5) by separation of variables. This gives the following expression:

$$\tilde{x}^{\lambda_-} = K\tilde{y}^{\lambda_+},$$

where K is a constant, such that every orbit corresponds to a value of K. Now, rewriting this in u and p then results in:

$$\left(\frac{\varepsilon}{\lambda_+}\left(u - \frac{\varepsilon\sqrt{\varepsilon}}{\delta}\right) + \frac{\varepsilon}{\lambda_-}p\right)^{\lambda_-} = K\left(u + p - \frac{\varepsilon\sqrt{\varepsilon}}{\delta}\right)^{\lambda_+}, \tag{5.6}$$

which is a cumbersome expression. Firstly, because of the exponents which are not in $\mathbb{Z}$, and secondly because it is not yet clear for which values of K the orbits on $\mathcal{A}$ are described. Unfortunately, no good solution for this problem was found. For example, a leading order description of the system didn't give any more quantitative information on the system.

We use a more geometric approach to overcome the complications caused by our attempt to directly follow the analysis from [3].

5.2 GEOMETRIC APPROACH

In this section, a geometric approach for the construction and proof of existence of periodic orbits will be performed. In doing so, we will use several qualitative aspects of the dynamical system. These can be derived from the phase plane and the system (3.1) right away.

From figures 3.2 and 4.1 it is clear what sort of behavior the orbits on $\mathcal{A}$ must display. It was determined that P is a saddle point on $\mathcal{M}$. Hence, the behavior of orbits near P and its stable and unstable manifold is known. Also, the nullclines can be determined. At $p = 0$, $u_\xi = 0$, so $p = 0$ is a nullcline. From the orientation of the flow at $\ell^{s,u}$ it can therefore be argued that the u-direction is negative for $p < 0$ and positive for all $p > 0$.
Moreover, to leading order the orbits on $\mathcal{A}$ have a vertical behavior in the sense

of reduced flow on $\mathcal{M}$. This can be concluded from (3.1). Because of our choice of $\delta = \varepsilon^\mu$ with $\mu > \frac{3}{2}$, it can be seen that the derivative of p is of order $\mathcal{O}(\varepsilon^2)$. However, the derivative of u is clearly of $\mathcal{O}(\varepsilon)$. This describes that the ratio u_ξ/p_ξ is of order $\mathcal{O}(\varepsilon^{-1})$, making it very large.

We will now start with a geometrical construction by which a proof for existence of periodic orbits at the end of this section can be derived from. The construction will be strongly based on figures 5.1 to 5.2.

5.2.1 Construction

Orbits with a negative p-value within $\mathcal{A}$ take off from T_o to make a fast excursion. In the left half-plane, this take-off curve admits a limited range of u-values. Define the interval I_1 as:

$$I_1 := \left\{ u \in \mathbb{R}_{>0} : \frac{1}{2}\varepsilon\left(c - \sqrt{c^2+4a}\right) \leq \frac{1}{2}\varepsilon\left(su - \frac{6b\sqrt{b}}{u}\right) \leq 0 \right\}, \tag{5.7}$$

which is also denoted in figure 5.1. The interval I_1 represents all u-values for which the corresponding p-value on T_o lies between the u-axis and the unstable manifold ℓ^u, see (3.4) and (3.19). This is the u-range for which orbits in $\mathcal{A}$ can take off for a fast excursion.

As mentioned before, in the construction of T_o and T_d, it was shown that the u-component is constant during this fast excursion. This results in the fact that the orbits that start in $\mathcal{A}$ will touch down in a certain range of u-values on the touch-down curve. This means that, regarded from the right half-plane with $p > 0$, only this part of the curve T_d can serve as a touch-down point for a periodic orbit. In the right half-plane there is therefore a range of candidates of periodic orbits, corresponding to this range of touch-down points. This is depicted in figure 5.1 as $U \cap T_d$. The touch-down points in the right half-plane, $p > 0$, account for unbounded orbits if the p value is larger than the p-value of ℓ^s[1], i.e. if this value lies outside of $\mathcal{A}$. These orbits cannot correspond to periodic orbits and should therefore be excluded. Define I_3 as:

$$I_3 := \left\{ u \in R_{>0} : \frac{1}{2}\varepsilon\left(su + \frac{6b\sqrt{b}}{u}\right) \leq \frac{1}{2}\varepsilon\left(c + \sqrt{c^2+4a}\right) \right\}, \tag{5.8}$$

which means that I_3 contains all u-values for which the corresponding p-value on T_d is smaller than the constant representing the leading order approximation of the stable manifold ℓ^s. See (3.20) and (3.4).

Next define I_2 as :

$$I_2 = I_3 \cap I_1, \tag{5.9}$$

which represents all u-values within $\mathcal{A}$ for which it is a priori possible to make an excursion through the fast field and return to $\mathcal{M}$. Moreover, these are the only candidates for periodic orbits with slow/fast behavior.

For notational purposes, introduce u_1, u_2, u_3, u_4 such that $I_1 = [u_1, u_2]$ and $I_2 = [u_3, u_4]$. The value of u_1 can be determined explicitly as the intersection point of T_o and ℓ^u. This yields:

$$u_1 = \frac{1}{2s}\left(c - \sqrt{c^2+4a} + \sqrt{(c-\sqrt{c^2+4a})^2 + 24sb\sqrt{b}}\right).$$

[1] This p-value is the same for all points in ℓ^s because this is a straight line to leading order.

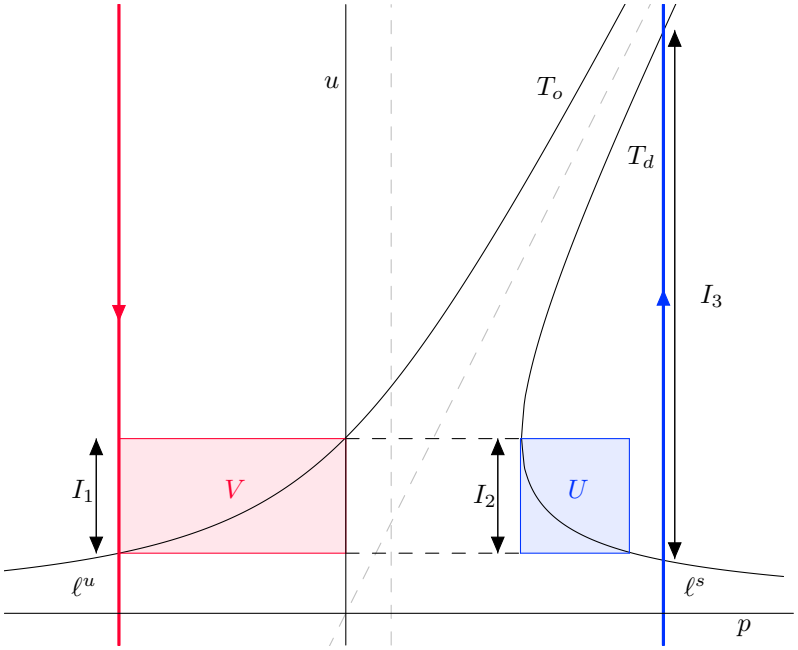

Figure 5.1: Schematic picture of $\mathcal{M}$ for $su_1 < c$. The orbits that take off at some point in $V \cap T_o$ will touch down at the corresponding value in $U \cap T_d$. No orbits will touch down in the unbounded area outside $\ell^{s,u}$. The gray dashed lines are the symmetry axes $p = c$ and $p = su$ of $\ell^{u,s}$ and $T_{o.d}$ respectively. The interval I_1 is the interval of values of u corresponding to $T_o \cap \mathcal{A} \cap \{p \leq 0\}$. The interval I_3 is the interval of values of u corresponding to $T_d \cap \mathcal{A} \cap \{p \geq 0\}$. The iterval $I_2 = I_3 \cap I_1$.

The value of u_2 is determined by the intersection of T_o and $p = 0$. From this it follows that:

$$su_2 = \frac{6b\sqrt{b}}{u_2} \tag{5.10}$$

$$u_2^2 = \frac{6b\sqrt{b}}{s}. \tag{5.11}$$

This of course yields two solutions but only one is valid since we consider the upper half-plane where $u \geq 0$.
Next, we will show that u_4 is always at the extremum[2] of the touch-down curve, as is depicted in Figure 5.1 and that $u_2 = u_4$ as a consequence.
For the extremum of T_d it holds that:

$$\frac{d}{du}\left(su + \frac{6b\sqrt{b}}{u}\right) = 0,$$

so

$$s - \frac{6b\sqrt{b}}{u_4^2} = 0 \tag{5.12}$$

$$\frac{6b\sqrt{b}}{s} = u_4^2 \tag{5.13}$$

This is the same result as for u_2 and with the same reasoning it holds that u_4 corresponds to the positive square root. Now $I_2 \subset I_1$ by definition and thus in particular $u_4 \leq u_2$. Since u_2 corresponds to a minimum of T_d (as function of p), it follows that I_3 necessarily extends beyond I_2. Thus we may conclude that indeed $u_4 = u_2$. From this it follows that the representation in the figures 5.1 to 5.2 are valid. This also yields that T_d is monotone on this interval. Moreover, it implies that I_2 is an empty set if and only if I_3 is an empty set, because I_3 vanishes exactly at this extremum, see Figure 4.2.

Note that in chapter 4, a condition was derived for the intersection of ℓ^s and T_d; for periodic orbits, the same condition, (4.5), must hold.

Depending on the position of ℓ^s, the values of u_1 and u_3 can either be equal or not. Three possible configurations are distinguished, corresponding to figures 5.1, 5.7 and 5.2. As c or s changes, the position of $\ell^{s,u}$ as opposed to $T_{o,d}$ modifies. As c decreases, the symmetry axis of $\ell^{s,u}$, which is $p = u$, will move towards the u-axis and with that there will be a point where $\ell^s \cap T_d$ has the same u-value as u_1. This corresponds to figure 5.2. If c increases even further, we arrive at figure 5.7, but this situation will be analyzed thoroughly in Section 5.3.

Of course one can imagine that if c decreases even further the u-value of $\ell^s \cap T_d$ will be larger than u_1, see figure 5.7 in the next section. As a consequence, this would result in the situation where $I_1 \neq I_2$. The transition point of $I_1 = I_2$ (when c is large enough) to $I_1 \neq I_2$ can be quantified.
The take-off and touch-down curves are symmetric around $p = su$. Because u_1 is a u-value on T_o, the value of u_3 can be obtained by reflecting u_1 in the line $p = su_1$.

Note that, the stable and unstable manifolds $\ell^{s,u}$ are symmetric around the line $p = c$. Therefore on the transition point, the intersection of T_d and ℓ^s is the reflection of u_1 around $p = c$. This signifies that for the transition point, where

[2] Extremum in the sense of p.

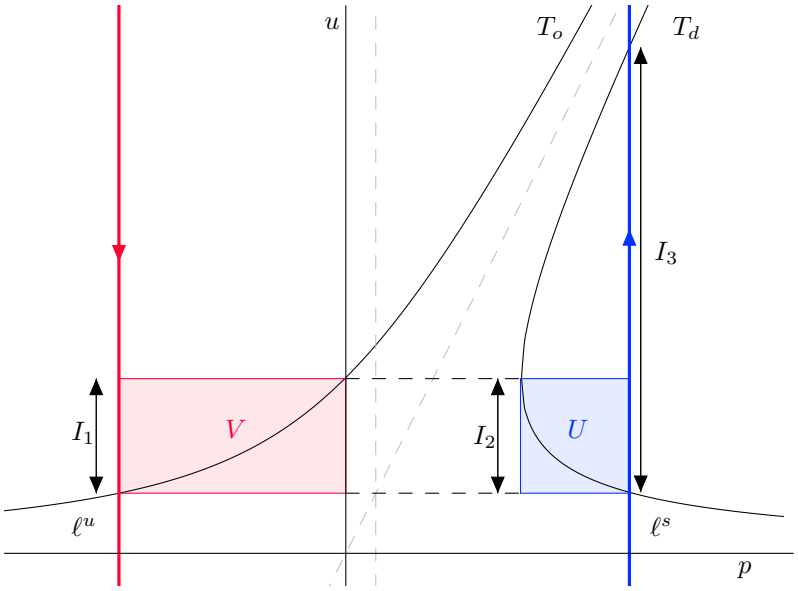

Figure 5.2: Schematic picture of $\mathcal{M}$ for $su_1 = c$. The orbits that take off at some point in $V \cap T_o$ will touch down at the corresponding value in $U \cap T_d$. No orbits will touch down in the unbounded area outside $\ell^{s,u}$. This represents the bifurcation point where periodic orbits originate.

u_1 is the u-value of the intersection of T_o and ℓ^u, it must hold that these axes of symmetry must coincide, i.e.

$$su_1 = c. \tag{5.14}$$

This is the transition which is depicted in figure 5.2. The dashed gray lines represent the symmetry axes and in figure 5.2 they intersect with u-value equal to u_1. It follows from this that for $su_1 \leq c$ we have $I_2 = I_1$ where for $su_1 < c$ the situation is as in Figure 5.1. In this section the situation where $I_2 = I_1$ will be discussed. In the next section the case that $su_1 > c$ will be analyzed. Then $I_1 \neq I_2$ which corresponds to figure 5.7.

To show the existence of periodic orbits, first some definitions and notations need to be introduced. For the proof of the existence of periodic orbits, we will define and restrict to the sets V, U and W, and it will become clear that this is enough. They follow naturally from the geometric construction in this section.

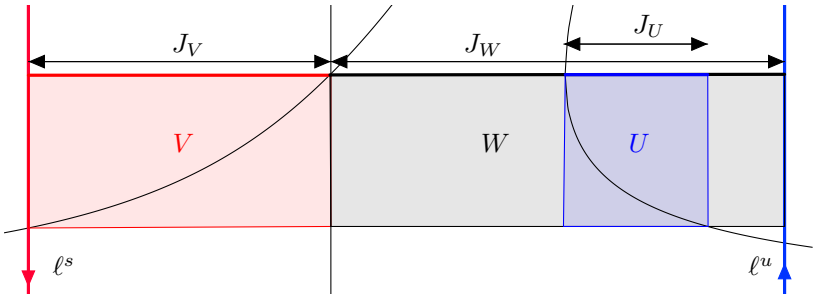

Figure 5.3: Detail of figure 5.1. Here, the set W is also depicted, in black. The intervals $J_{U,V,W}$ are intervals in the p-range of $\mathcal{A}$.

The set V is defined as:

$$V = \left\{(u,p) \in I_1 \times \left[\frac{1}{2}\varepsilon\left(-c + \sqrt{c^2+4a}\right), 0\right]\right\}, \tag{5.15}$$

and the set U is defined as:

$$U = \left\{(u,p) \in I_2 \times \left[\frac{1}{2}\varepsilon\left(su_4 + \frac{6b\sqrt{b}}{u_4}\right), \frac{1}{2}\varepsilon\left(su_3 + \frac{6b\sqrt{b}}{u_3}\right)\right]\right\}, \tag{5.16}$$

which are depicted in figure 5.1. Moreover, define W as:

$$W = \left\{(u,p) \in I_2 \times \left[0, \frac{1}{2}\varepsilon\left(c + \sqrt{c^2+4a}\right)\right]\right\}. \tag{5.17}$$

These sets are represented in figure 5.3.

Periodic orbits that touch-down near manifold $\mathcal{M}$ in U will eventually return to V. We know this because of the character of the fixed point P and the fact that the area $\mathcal{A}$ is invariant. One should regard V, U, W as sets of parts of orbits in $\mathcal{A}$.

Because $\ell^{s,u}$ are in particular the stable and unstable manifolds of P, we know that these are 'attached' to P, which lies on the $p-$axis. Because of everything we know now about $\mathcal{A}$, we know that *every* orbit intersecting W must eventually cross the p-axis and pass through area V. The same reasoning, with backwards flow, holds for every orbit in V. Introduce intervals $J_{U,V,W}$ as:

$$\begin{aligned} J_V &:= V \cap \{u = u_2\}, \\ J_W &:= W \cap \{u = u_2\}, \\ J_U &:= U \cap \{u = u_2\}. \end{aligned}$$

These are just p-intervals and closed subsets of $\mathbb{R}$, and depicted in figure 5.3. They could be seen as the p-values of the orbits in V, W, U when they pass through the line $\{u = u_2\}$. Note that $J_V \cup J_W = \{u = u_2\} \cap \mathcal{A}$ and $J_U \subset J_W$.
On the sets $\{u = u_2\} \cap \mathcal{A}$ there exists a natural norm induced by the norm on $\mathbb{R}$. Note again that the orbits on $\mathcal{A}$ are vertical to leading order.

Assume $\gamma(\xi)$ to be an orbit on $\mathcal{A}$ with a nonzero intersection with J_W. Define the map $\mathcal{S}$ as:

$$\mathcal{S} : J_W \to J_V, \quad \gamma(\xi) \cap J_W \mapsto \gamma(\xi) \cap J_V.$$

It assigns to the intersection point of an orbit with J_W its intersection point with J_V. It was argued above that $\mathcal{S}$ is surjective, because all orbits starting in W must

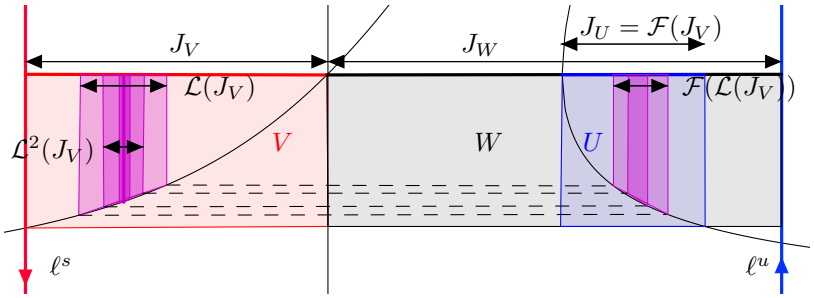

Figure 5.4: Depiction of iterations of $\mathcal{L}$. Actually the intervals $\mathcal{L}(J_V)$, $\mathcal{F}(\mathcal{L}(J_V))$, and $\mathcal{L}^2(J_V)$ are subsets of J_V, but for clarity they are indicated differently. The purple areas are the areas that arise in the construction of $\mathcal{F}(J_V)$, $\mathcal{L}(J_V)$ etc.

eventually intersect V. It is also injective because orbits cannot intersect. This means that the map $\mathcal{S}$ is bijective.

Next, we define a second map $\mathcal{F}$ which assigns to the intersection of an orbit with J_V its counterpart in J_U after an excursion through the fast field.

Assume $\zeta(\xi)$ to be an orbit with a nonempty intersection with J_V.

$$\mathcal{F} : J_V \to J_U, \quad \zeta(\xi) \cap J_V \mapsto \zeta(\xi) \cap J_U.$$

One can view $\mathcal{F}$ as:

$$\mathcal{F} = (\pi_U)^{-1} \circ \psi \circ \pi_V,$$

where ψ is a map from base point $w^- \in T_o$ to base point $w^+ \in T_d$ associated to the orbit homoclinic to $\mathcal{M}$ that jumps off from $\mathcal{M}$ in $\pi_V(w) \in T_o$ - where $w \in J_V$ - and touches down on $\mathcal{M}$ in $\pi_U(\mathcal{F}(w)) \in T_d$[3]. The maps $pi_{U,V}$ are given as:

$$\pi_V : J_V \to T_o, \quad \tilde{p} \mapsto \{p = \tilde{p}\} \cap T_o \qquad \text{assigns the take-off point.} \tag{5.18}$$

$$\pi_U : J_U \to T_d, \quad \tilde{p} \mapsto \{p = \tilde{p}\} \cap T_d \qquad \text{assigns the touch-down point.} \tag{5.19}$$

Actually, π_V is a map which assigns to an orbit $\zeta(\xi)$ a base point w^- in $T_o \cap V$ such that there is a ξ^- for which $\zeta(\xi^-) = w^-$. Similarly, π_U is a map which assigns to an orbit $\zeta(\xi)$ a base point w^+ in $T_d \cap U$ such that there is a ξ^+ for which $\zeta(\xi^+) = w^+$.

The map $\mathcal{F}$ is injective, because when it is assumed that $\mathcal{F}x_1 = \mathcal{F}x_2$, then this means that they have the same touch-down point and therefore necessarily the same take-off point. But this means that they are the same orbit because orbits cannot intersect, so $x_1 = x_2$. By construction of U, the map $\mathcal{F}$ is surjective, so it is bijective.

Next introduce the return map $\mathcal{L}$ as the composition of $\mathcal{S}$, restricted to $J_U \subset J_W$, and $\mathcal{F}$.

$$\mathcal{L} : J_V \to J_V, \quad \mathcal{L} = \mathcal{S} \circ \mathcal{F}. \tag{5.20}$$

It is defined for every orbit in the left half-plane of $\mathcal{A}$ because it assigns to its intersection with J_V its intersection with J_V after making a fast excursion and a slow trajectory through $\mathcal{A}$. This map is a Poincaré map, see [5], and hence a periodic orbit is indicated by a fixed point of $\mathcal{L}$. Some iterations of the Poincaré map $\mathcal{L}$ are depicted in figure 5.4. In subsection 5.2.2 it will be verified that the iterations show contractive behavior and that this implies a fixed point of the Poincaré map.

[3]The definition of a base point was given in Section 3.4.

5.2.2 Contraction map

What we would like to show is that $\mathcal{L}$ is has a fixed point. One way to approach this, is to show that $\mathcal{L}$ is a contraction mapping and then use Banach's Fixed Point Theorem, see Theorem 6. It can indeed be shown that $\mathcal{L}$ is a strong contraction and this will be done by considering $\mathcal{S}$ and $\mathcal{F}$ separately. For this a definition of strong contraction is needed.

Definition 2. Suppose (X, d) is a metric space. A map $f : X \to X$ is called a *contraction* on X if and only if there exists $k \in [0, 1]$ such that

$$d(f(x), f(y)) \leq kd(x, y)$$

for all $x, y \in X$ If $k \in [0, 1)$, the map f is called a *strong contraction.*

A contraction property for $\mathcal{F}$ will be shown first. For this, Cauchy's Mean-Value theorem, also known as the Generalized Mean-Value theorem, will be used [1].

Theorem 5 (Cauchy's Mean-Value theorem)**.** *If functions f and g are both continuous on $[a, b]$ and differentiable on (a, b), and if $g'(x) \neq 0$ for every x in (a, b), then there exists a number $c \in (a, b)$ such that:*

$$\frac{f(b) - f(a)}{g(b) - g(a)} = \frac{f'(c)}{g'(c)}.$$

For a proof of this theorem, see [1]. This theorem will be applied to T_o and T_d which are considered as functions of u with domain I_1. On I_1, both $T_o(u)$ and $T_d(u)$ are continuous and differentiable. The derivatives are given as:

$$\frac{\partial}{\partial u} T_o = \frac{1}{2}\varepsilon \left(s + \frac{6b\sqrt{b}}{u^2} \right),$$
$$\frac{\partial}{\partial u} T_d = \frac{1}{2}\varepsilon \left(s - \frac{6b\sqrt{b}}{u^2} \right),$$

which are both nonzero on the interior of I_1. For any interval $[u_1, u_2] \subset I_1$ it holds then that there exists a $c \in [u_1, u_2]$ such that:

$$T_d(u_2) - T_d(u_1) = \frac{T_d'(c)}{T_o'(c)} \left(T_o(u_2) - T_o(u_1) \right).$$

The absolute value is a natural metric in this case, so consider:

$$|T_d(u_2) - T_d(u_1)| = \left| \frac{T_d'(c)}{T_o'(c)} \right| |T_o(u_2) - T_o(u_1)|. \tag{5.21}$$

But $\left| \frac{T_d'(c)}{T_o'(c)} \right|$ can be estimated. It holds that

$$\left| \frac{T_d'(c)}{T_o'(c)} \right| = \left| \frac{s - \frac{6b\sqrt{b}}{c^2}}{s + \frac{6b\sqrt{b}}{c^2}} \right| = \frac{\left| s - \frac{6b\sqrt{b}}{c^2} \right|}{\left| s + \frac{6b\sqrt{b}}{c^2} \right|}.$$

Applying the triangle inequality yields

$$\frac{\left| s - \frac{6b\sqrt{b}}{c^2} \right|}{\left| s + \frac{6b\sqrt{b}}{c^2} \right|} \leq \frac{|s| + \left| \frac{6b\sqrt{b}}{c^2} \right|}{\left| s + \frac{6b\sqrt{b}}{c^2} \right|}.$$

However, the equality can only hold if either s or $\frac{6b\sqrt{b}}{c^2}$ is negative, which is never the case. Therefore:

$$\frac{\left|s - \frac{6b\sqrt{b}}{c^2}\right|}{\left|s + \frac{6b\sqrt{b}}{c^2}\right|} < \frac{|s| + \left|\frac{6b\sqrt{b}}{c^2}\right|}{\left|s + \frac{6b\sqrt{b}}{c^2}\right|}. \tag{5.22}$$

And again because it is known that $s > 0$ and $\frac{6b\sqrt{b}}{c^2} > 0$ it holds that:

$$|s| + \left|\frac{6b\sqrt{b}}{c^2}\right| = \left|s + \frac{6b\sqrt{b}}{c^2}\right| = s + \frac{6b\sqrt{b}}{c^2}.$$

And hence:

$$\frac{|s| + \left|\frac{6b\sqrt{b}}{c^2}\right|}{\left|s + \frac{6b\sqrt{b}}{c^2}\right|} = \frac{s + \frac{6b\sqrt{b}}{c^2}}{s + \frac{6b\sqrt{b}}{c^2}} = 1. \tag{5.23}$$

Combining (5.22) and (5.23) yields:

$$\left|\frac{T_d'(c)}{T_o'(c)}\right| < 1.$$

Then it holds that (5.21) becomes a contraction property for a map from T_o to T_d. By construction, it holds that for fixed interval $[u_1, u_2]$ there exists a $k \in [0, 1)$ such that

$$|T_d(u_2) - T_d(u_1)| = k\,|T_o(u_2) - T_o(u_1)|\,,$$

which $k = \left|\frac{T_d'(c)}{T_o'(c)}\right|$. A uniform bound k_f for every interval $[u_1, u_2] \subset I_1$ can be defined as

$$k_f := \max_{c \in I_1} \left|\frac{T_d'(c)}{T_o'(c)}\right|.$$

This is welldefined because I_1 is a bounded interval, and the function $T_d'(u)/T_o'(u)$ admits both a maximum and a minimum value on bounded intervals. Moreover, k_f is still strictly smaller than 1. The map $\mathcal{F}$ maps from J_V to J_U via T_o and T_d. For ψ it now holds that

$$|\psi\pi_V(u_1) - \psi\pi_V(u_2)| \leq k_f|u_1 - u_2|.$$

By construction of $\mathcal{F}$ it then holds that:

$$|\mathcal{F}u_1 - \mathcal{F}u_2| \leq k_f|u_1 - u_2|. \tag{5.24}$$

Which makes $\mathcal{F}$ a strong contraction.

A similar property holds for $\mathcal{S}$. We know that the two ends of J_W, which are $x_1 := p = 0$ and $x_2 := p = \frac{1}{2}\varepsilon\left(c + \sqrt{c^2 + 4a}\right)$ are mapped to $p = 0$ and $p = \frac{1}{2}\varepsilon\left(c - \sqrt{c^2 + 4a}\right)$ respectively, the ends of J_V. Note that because $\ell^{s,u}$ are symmetric around $p = c$ and $c > 0$, it holds that:

$$|x_1 - x_2| > |\mathcal{S}(x_1) - \mathcal{S}(x_2)|.$$

Which means that all orbits from W are at least squeezed into a smaller region V because orbits cannot intersect. However, this proves the contraction condition just for a special pair of elements in J_W. What we need to show is that for every pair of orbits, the distance of the images is strictly smaller than the distance of the originals. For this, we need a small intermezzo on dynamics in a linear system with a saddle fixed point.

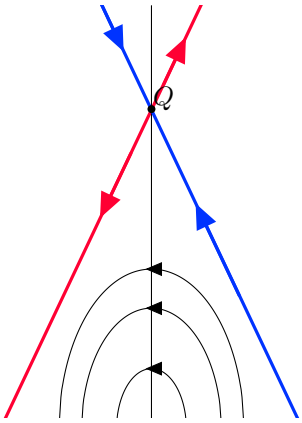

Figure 5.5: The (y, x) phase plane of the symmetric system considered in the intermezzo. The orbits are symmetric for $y \to -y$. The stable and unstable manifold are depicted in blue and red respectively.

INTERMEZZO

Consider a dynamical system:

$$x' = x - 1,$$
$$y' = -y.$$

Then this system has a saddle fixed point at $Q = (x, y) = (1, 0)$. Moreover, the system is symmetric for $y \to -y$, and the phase plane looks like figure 5.5. This means that for every orbit on the left half-plane, there exists a counterpart in the right half-plane. Note that the slow system that is considered here, (3.1), is also linear but stretched and twisted such that the phase plane looks qualitatively like figure 5.6. Therefore a linear transformation can get the system of interest, (3.1), into a system that has a phase plane like figure 5.5.
It follows that for system (3.1) it must hold that the orbits are 'squeezed evenly' from the right half-plane of $\mathcal{A}$ to the left half-plane. In other words, there is a linear stretching because it is a linear transformation of a symmetric system.

From the intermezzo, it can now be concluded that if one special pair of orbits gets contracted by $\mathcal{S}$, this must hold for all pairs of orbits from W. The fact that system (2.4) can be transformed into a symmetric system by a linear transformation, yields that the phase plane must stretch linearly. Therefore, the contraction property must especially hold for every pair of orbits in U. Since the ratio by which x_1 and x_2 get contracted is known, it can be concluded that for every p_1, p_2 which are elements of J_W:

$$|\mathcal{S}p_1 - \mathcal{S}p_2| \leq k_s |p_1 - p_2|, \tag{5.25}$$

and this k_s can be quantified. It is equal to the width of V divided by the width of W, because this is the maximum contraction rate.

$$k_s := \frac{\frac{1}{2}\varepsilon\left(c - \sqrt{c^2 + 4a}\right)}{\frac{1}{2}\varepsilon\left(c + \sqrt{c^2 + 4a}\right)} < 1.$$

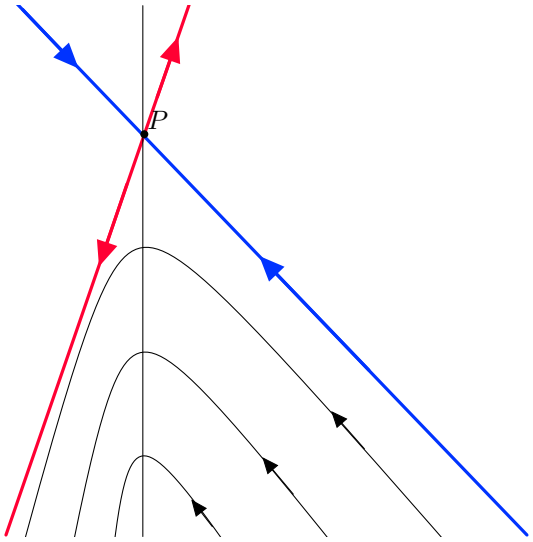

Figure 5.6: A qualitative phase plane of (3.1), without symmetry. The stable and unstable manifold are depicted in blue and red respectively.

Combining the results of $\mathcal{F}$ and $\mathcal{S}$ yields that for all p_1, p_2 which are the p-coordinates of the intersection of two orbits in $\mathcal{A}$ with J_V:

$$\begin{aligned} |\mathcal{L}p_1 - \mathcal{L}p_2| &= |\mathcal{S}\mathcal{F}p1 - \mathcal{S}\mathcal{F}p2|, \\ &\leq k_s|\mathcal{F}p_1 - \mathcal{F}p_2|, \\ &\leq k_s k_f |p_1 - p_2|, \end{aligned}$$

because of (5.24) and (5.25). Since $k_s, k_f < 1$, the map $\mathcal{L}$ is a strong contraction.

Remark 3. In this chapter some leading order approximations are used. Since $|1 - k_s k_f| = \mathcal{O}(1)$[4], an $\mathcal{O}(\varepsilon)$ has no impact on our main arguments. However, it is also used that the orbits are vertical to leading order. This statement holds for as long as $p = \mathcal{O}(1)$, p cannot get too close to the u-axis. The construction above is therefore valid for $p \gg \varepsilon$. ◀

5.2.3 Proof of existence

In this subsection, a proof for the existence of periodic orbits will be given. Part of this proof relies on the construction of the slow part of the periodic orbit as a fixed point of the Poincaré map. However, this is not the full construction of the periodic orbit. The take-off and touch-down curves that were constructed in Section 3.4 were constructed for orbits homoclinic to $\mathcal{M}$. A periodic orbit with a slow/fast structure must exit a neighborhood of $\mathcal{M}$ once *every* period, so it cannot be homoclinic to $\mathcal{M}$.

The map $\mathcal{S} : J_U \to J_V$ restricted to J_U yields by definition a set $J^1 \subsetneq J_V$, where $J^1 = \mathcal{S}(J_U)$. By construction of $\mathcal{L}$ it holds that $\mathcal{L}(J_V) = J^1$. Introduce:

$$J^i = \mathcal{L}^i(J_V), \quad i = 1, 2, \ldots$$

[4]It is easily verified that the expressions for k_s and k_f do not contain any ε.

Because $\mathcal{L}$ is a contraction, it holds that:

$$J_V \supset J^1 \supset J^2 \ldots,$$

therefore, we aim at applying the following theorem from [9].

Theorem 6 (Banach's fixed point theorem)**.** *Suppose (X, d) is a non-empty complete metric space and $f : X \to X$ is a strong contraction with Lipschitz constant $k \in (0, 1)$. Then f has a unique fixed point in X and, for each $w \in X$, the sequence $(f(w))^n$ converges to this point.*

For a proof of this theorem, see [9] or other books on metric spaces.

With this theorem, a new theorem on the existence of periodic orbits can be formulated.

Theorem 7. *Assume s and c are given such that $0 < su_1 < c$, where u_1 is the intersection point of T_o and ℓ^u, i.e. assume that s and c are given such that:*

$$\frac{1}{2}\left(c - \sqrt{c^2 + 4a} + \sqrt{(c - \sqrt{c^2 + 4a})^2 + 24sb\sqrt{b}}\right) < c.$$

Then there exists an ε_0 such that for all $\varepsilon < \varepsilon_0$ there exists a unique periodic orbit with a slow/fast structure in system (2.4).

The condition that $0 < su_1 < c$ means that $s > 0$, which corresponds to patterns traveling *uphill*, and $I_1 = I_2$. This is the distinction between figures 5.1 and 5.2. It will become clear in Section 5.3 that this condition is essential for the existence of periodic orbits.

Proof. Consider the operator $\mathcal{L}$ which was defined above. It was already shown that there exists a $k \in [0, 1)$ such that the contraction condition holds. It is obvious that this $k \neq 0$. Moreover, the closed interval J_V is complete with the euclidian norm on $J_V \subset \mathbb{R}$. This means that Banach's Fixed-Point Theorem applies and therefore $\mathcal{L}$ has a fixed point.

The fixed point of $\mathcal{L}$ corresponds to a point in J_V which is mapped by $\mathcal{L}$ to itself. This point corresponds to an orbit with two parts on $\mathcal{M}$ and an excursion through the fast field in $W^s(\mathcal{M}) \cap W^u(\mathcal{M})$. Note that, because this orbit lies *within* both the stable and unstable manifold of $\mathcal{M}$, it is homoclinic to $\mathcal{M}$ and therefore by definition not a periodic orbit. Define this orbit as $\Gamma_h(\xi)$ and $\Gamma_{h,\mathcal{M}}(\xi)$ as the slow part of this orbit on $\mathcal{M}$, which was obtained by Banach's fixed point theorem. To be more precise, suppose that the initial value $\Gamma_{h,\mathcal{M}}(0)$ is at its maximum u-value $u_{\max}$, then $\Gamma_{h,\mathcal{M}}$ is obtained by flowing $\Gamma_{h,\mathcal{M}}(0)$ forward up to its intersection with T_o and backward up to its intersection with T_d.

It will now be shown that this $\Gamma_h(\xi)$ gives rise to the existence of a periodic orbit described in the theorem statement. In doing so, a line segment $\jmath$ of points $(u_{\max}, 0, v, q^*)$ will be defined. The fixed value q^* corresponds to the q-value of the maximum of the v-pulse. To leading order, this is equal to 0, but there can be an exponentially small perturbation to this, which cannot be noticed by a leading order analysis.

Note that $\mathcal{M}$ is invariant, and that an orbit homoclinic to $\mathcal{M}$ must touch down closer to $\mathcal{M}$ than an periodic orbit, because a periodic orbit must make the fast excursion again and has to leave an $\mathcal{O}(\varepsilon)$ neighborhood of $\mathcal{M}$.
The line segment will be determined in such a way that when this line segment is considered a set of initial conditions, the orbits it generates remain close to $\Gamma_h(\xi)$.

This means that the length of $\jmath$ must be determined in such a way that all orbits with initial values on $\jmath$ remain close to $\mathcal{M}$ up to the take-off point of $\Gamma_h(\xi)$. Because $u_{\max}$ is near P, it has a magnitude of $\mathcal{O}(\frac{\varepsilon\sqrt{\varepsilon}}{\delta})$ or $\mathcal{O}(\varepsilon^{\frac{3}{2}-\mu})$. Since the eigenvalues of the slow dynamics in system (2.4) have a magnitude $\mathcal{O}(\varepsilon^{\mu+\frac{1}{2}})$, the orbits with initial value of $\mathcal{O}(\varepsilon^{\frac{3}{2}-\mu}$ take an $\mathcal{O}(\varepsilon^{-2\mu+1}$ amount of time (measured in ξ) to travel from $u = u_{\max}$ to the neighborhood of the take-off point, which is $\mathcal{O}(1)$.
The dynamics of v in (2.4) is linear and therefore the flow of v is exponential. The eigenvalues of the fast dynamics in (2.4) are $\mathcal{O}(1)$. The magnitude of v must remain small (i.e. $\ll 1$) for an $\mathcal{O}(\varepsilon^{-2\mu+1})$ amount of time, so the length of $\jmath$ will be:

$$\jmath = (u_{\max}, 0, v, q^*), \text{with} \quad v \in \left(K_1 e^{-(k/\varepsilon^{2\mu-1})}, K_2 e^{-(k/\varepsilon^{2\mu-1})}\right),$$

with $K_1 < K_2, k > 0$ and K_1 sufficiently small and K_2 sufficiently large. Now, $\jmath$ is determined as a set of initial values for orbits that remain close to $\Gamma_h(\xi)$, even after its take-off point. More specifically, these orbits have a take-off point close to the take-off of $\Gamma_h(\xi)$.

Define the u value of the point where $\Gamma_h(\xi)$ intersects with T_o to be $\tilde{u}$.
Consider the two-dimensional manifold $\mathcal{J}$ composed by flowing initial conditions on $\jmath$. The constants K_1, K_2 and k are chosen appropriately such that some of these 'exit points' have a u value larger than $\tilde{u}$ and some have a u value smaller than $\tilde{u}$. At these exit points, $\mathcal{J}$ is $\mathcal{O}(e^{-(\tilde{k}/eps^{2\mu-1})}$ close to the subset $W^u(\Gamma_{h,\mathcal{M}})$ of $W^u(\mathcal{M})$ corresponding to base points in $\Gamma_{h,\mathcal{M}}$. This estimate follows from the proofs on existence of periodic orbits in [3] and [2] and references therein. The same holds for backward flow, such that $\mathcal{J}$ lies $\mathcal{O}(e^{-(\tilde{k}/eps^{2\mu-1})}$ close to $W^s(\Gamma_{h,\mathcal{M}})$ at points where this backwards flow leads orbits in $\mathcal{J}$ out of an $\mathcal{O}(\varepsilon)$ neighborhood of $\mathcal{M}$.

The take-off and touch-down curves were constructed such that $W^s(\mathcal{M})$ and $W^u(\mathcal{M})$ intersect transversely. A priori, it is not clear that $\mathcal{J}$ intersects itself. Because of the closeness estimates, it must also hold that $\mathcal{J}$ 'approaches' itself transversely. The two-dimensional strip constructed by flowing $\jmath$ forward and backward makes such a turn that if it intersects itself, it must be transversal. The intersection can be ensured by 'tuning' s with an exponentially small perturbation.

This intersection must be exponentially close to $\Gamma_h(\xi)$ by definition of $\mathcal{J}$. Because of the appropriate choices for K_1, K_2 and k and the fact that the intersections $T_o \cap \Gamma_{h,\mathcal{M}}$ and $T_d \cap \Gamma_{h,\mathcal{M}}$ are transverse, the intersection of $\mathcal{J}$ with itself is unique, and the periodic orbit as stated in the theorem lies inside of it. □

The question now arises what happens for parameter values such that $su_1 \geq c$. In the next section, it will be shown that in this case all orbits starting in V will eventually be mapped outside $\mathcal{A}$.

5.3 No periodic orbits

In the previous section it became clear that the contraction property of the map $\mathcal{L}$ is crucial for the existence of periodic orbits. The contraction was established knowing that $I_1 = I_2$, such that $\mathcal{F} : J_V \to J_U$ was a bijection. This need not be the case. In this section the behavior of map $\mathcal{L}$ for $su_1 > c$ will be considered. It will be proved that, as the title of the section already gives away, no periodic orbits can exist in this case. This ultimately leads to the existence of a bifurcation curve in the (s, c)-plane.

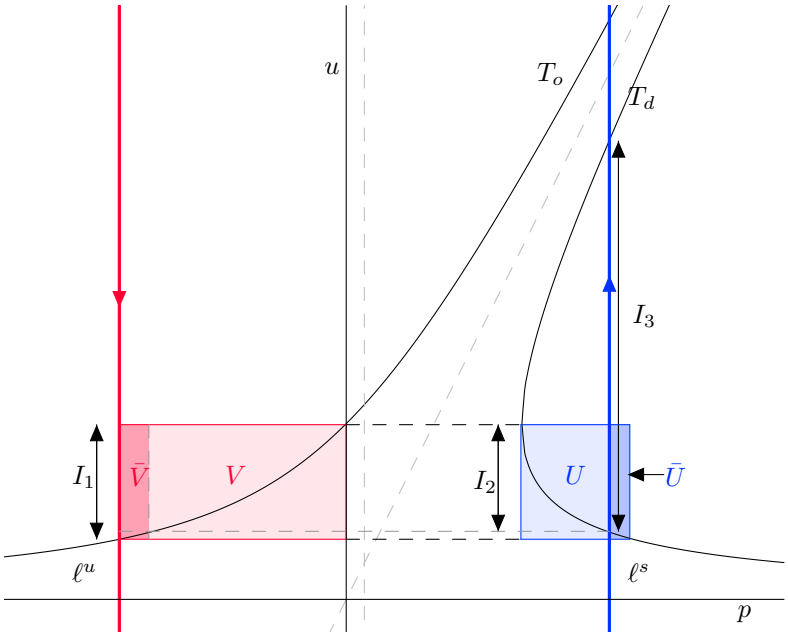

Figure 5.7: Schematic picture of $\mathcal{M}$ for $su_1 > c$. The orbits that take off at some point in $V \cap T_o$ will touch down at the corresponding value in either $U \cap T_d$ or $\bar{U} \cap T_d$. Orbits that touch down in $\bar{U}$ will never return into the area enclosed by $\ell^{s,u}$ and grow unboundedly. All orbits taking off in $\bar{V}$ touch down in $\bar{U}$.

For $su_1 > c$ the situation is as depicted in 5.7. This figure was constructed as follows. The area's U, V were defined in the previous section in (5.15) and (5.16). Next define $\bar{U}$ as:

$$\bar{U} := U \backslash \mathcal{A},$$

which represents the set of all points in U that are not in $\mathcal{A}$ and therefore are not part of bounded orbits on $\mathcal{M}$. Note that these points cannot be candidates for periodic orbits.
Also define $\bar{V}$ as:

$$\bar{V} := \mathcal{F}^{-1}(\bar{U}),$$

the pre-image of $\bar{U}$ under the map $\mathcal{F}$ which assigns base points in T_o to base points in T_d. In figure 5.7 there are dashed lines which explain how $\bar{V}$ was constructed from $\bar{U}$.

The interval $J_{\bar{U}}$ and $J_{\bar{V}}$ are defined analogous to $J_{U,V,W}$:

$$J_{\bar{U}} := \bar{U} \cap \{u = u_2\},$$
$$J_{\bar{V}} := \bar{V} \cap \{u = u_2\}.$$

It follows from this construction that in the situation where $su_1 > c$ we can formulate the following result.

Lemma 1. *Let (s, c) be given such that $su_1 > c$. Then there exist no periodic orbits with a slow-fast structure in* (2.4).

Proof. For the proof the maps $\mathcal{S}, \mathcal{F}$ defined in the previous section will be used again. Note that $\mathcal{F} : J_V \to J_U$ is still bijective.

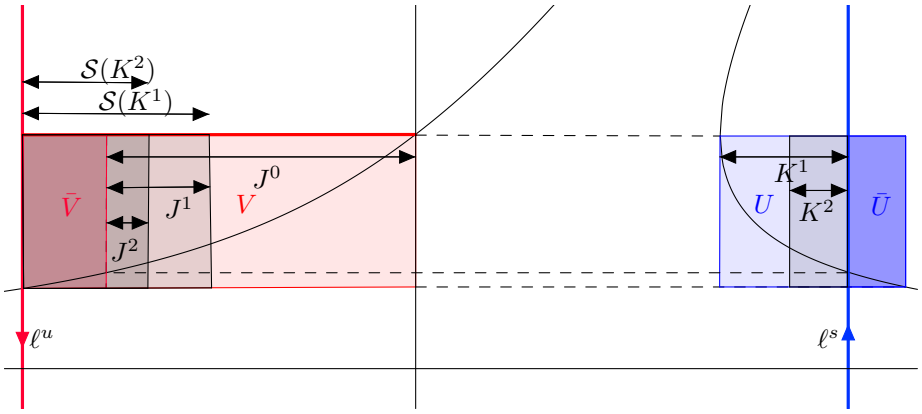

Figure 5.8: Schematic representation of two iterations of the map described in the proof of lemma 1. In gray, the iterations of V are depicted. The intervals $J^{0,1,2}$ and $K^{0,1}$ are actually subsets of J_V and J_U respectively, but for notational purposes it is displayed differently.

With an iterative procedure it will be shown that all orbits starting in J_V will eventually be mapped out of $\mathcal{A}$. The map $\mathcal{L}$ is no longer well-defined because $\mathcal{S}$ does not map $J_{\bar{U}}$ inside J_V. Instead of $\mathcal{L}$ we will work with an iteration in several steps.

Define:

$$\begin{aligned} K^i &= \mathcal{F}(J^{i-1}), \\ J^i &= \mathcal{S}(K^i) \backslash J_{\bar{V}}, \\ J^0 &= J_V \backslash J_{\bar{V}}, \end{aligned}$$

which seems tenuous at first, but which is clarified in figure 5.8.

The map $\widehat{\mathcal{L}}$ that sends J^i to J^{i+1} will be considered here, so $J^i \to J^{i+1}$ is said to be one iteration. The map $\widehat{\mathcal{L}}$ is again an Poincaré map.
Note that every orbit of $\widehat{\mathcal{L}}$ will end up in $J_{\bar{V}}$ at some point, will be mapped into $\bar{U}$ and is therefore no periodic orbit. These orbits must be excluded. We will define $J^i \to J^{i+1}$ as one iteration.

It was clear from the previous section that $\mathcal{S}, \mathcal{F}$ have a contraction property. This was shown considering the slow dynamics and $T_{o,d}$, which do not change when $su_1 > c$. The contraction properties must therefore still hold. As a consequence of that it holds that $K^i \subset K^{i-1}$ and

$$\mathcal{S}(K^i) \subsetneq \left(J^{i-1} \cup J_{\bar{V}}\right).$$

This yields that either $J^i \subsetneq J^{i-1}$ or $J^i = \emptyset$. If $J^i = \emptyset$ it is clear that all 'candidates' for periodic orbits starting in $J_V \backslash J_{\bar{V}}$ are mapped into $J_{\bar{V}}$ in i iterations. This already concludes that these cannot be periodic orbits.
If $J^i \subsetneq J^{i-1}$, another iteration can be performed. However, notice that the boundary between $J_{\bar{V}}$ and $J_V \backslash J_{\bar{V}}$ is the pre-image of $\ell^s \cap \{u = u_2\}$. This means that the interval J^i will be mapped to K^{i+1} which is then an interval containing $\ell^s \cap \{u = u_2\}$.
Moreover, every non-empty J^i will contain $\mathcal{F}^{-1}(\ell^s \cap \{u = u_2\})$, and therefore every K^{i+1} will contain $\ell^s \cap \{u = u_2\}$ and this means that $\mathcal{S}(K^{i+1})$ contains ℓ^u and $\mathcal{S}(K^{i+1})$ has a nonzero intersection with $J_{\bar{V}}$ again.

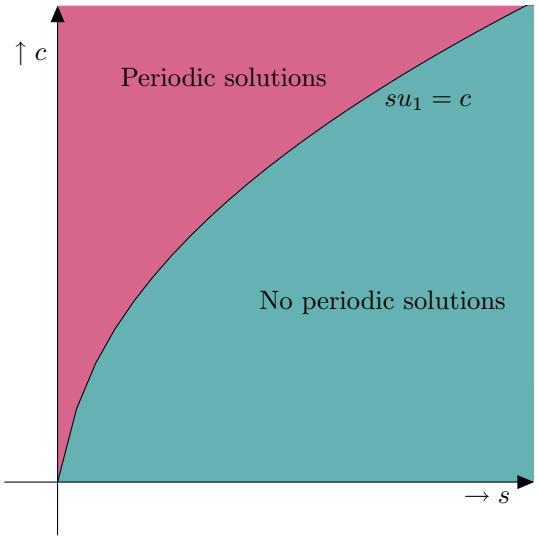

Figure 5.9: Bifurcation diagram in the (s, c)-plane. The curve above was drawn with $a = 1$ and $b = 2$ but the qualitative behavior is the same for all (a, b) values.

It follows that because $\forall K^i \neq \emptyset, \quad \ell^s \in K^i$ and because of the strong contraction property of $\mathcal{S}$, there is a certain i, which is finite, for which $J^i = \emptyset$. This is because $J_{\bar{V}}$ remains constant. As a result, all orbits starting in $J_V \backslash J_{\bar{V}}$ will be mapped out of $\mathcal{A}$ within at most i iterates.

Because of the construction of $\bar{V}$, this means that all orbits of $\widehat{\mathcal{L}}$ that intersect J_V will be mapped out of $\mathcal{A}$ within at most $i + 1$ iterates.

All bounded orbits of $\widehat{\mathcal{L}}$ must have a slow part that lies in $\mathcal{A}$ and all possible periodic orbits with a slow-fast structure on $\mathcal{A}$ must pass J_V, but from the construction above, it follows that there cannot exist any fixed points of $\widehat{\mathcal{L}}$. Since this is a Poincaré map, it follows that there cannot exist periodic orbits with a slow-fast structure in (2.4). □

5.3.1 Bifurcation

In the previous sections and theorem 7 and lemma 1 it was shown that depending on the values of s and c, periodic orbits do or do not exist. If $su_1 < c$, which corresponds to figure 5.1, there exists for any given c exactly one s such that there exists a periodic orbit with traveling wave speed s. Alternatively, if $su_1 > c$, these periodic orbits cannot exist, see figure 5.7.

Naturally, there is a transition curve between these two cases, which is given as $su_1 = c$. This is the situation that corresponds to figure 5.2. Note that it was already considered in section 5.2.3 because in this case $I_1 = I_2$. The transition curve is depicted in figure 5.9, the bifurcation diagram in the (s, c)-plane.

Theorem 7 cannot be applied to the transition point where $su_1 = c$ because $\mathcal{L}$ is not defined for this case. However, it can be regarded as approaching the limit point of the accumulation point of $\mathcal{L}$ as $su_1 \uparrow c$.

Because $\ell^s \cap U \neq \emptyset$ and $\ell^u \cap V \neq \emptyset$, and it is obvious that these are mapped into a small neighborhood of one another by $\mathcal{S}$ and $\mathcal{F}$. It follows that the accumulation point of the Poincaré map is on ℓ^u. The result of this observation is that at the

transition point, the periodic orbit that exists for all $su_1 < c$ collides with the homoclinic orbit.

From chapter 4, it was already determined that the homoclinic solution satisfies $su = c$ where u was the u-value for which the orbit makes the fast excursion. This corresponds completely with the results that were derived in the current chapter. So apart from the construction that was performed for the homoclinic orbit, this chapter provides an alternative geometric view on the existence of a homoclinic orbit.

5.4 Recap

It was mentioned at the beginning of this chapter that in [3], a range of parameter values for which periodic orbits can exist was presented. The two boundary points of this range correspond to a saddle node bifurcation and the homoclinic orbit. One can expect this to happen in system (1.4) as well. One of these boundary points was indeed found and corresponds to the homoclinic orbit. However, another boundary was not yet found.
In [3] the saddle node bifurcation corresponds to the slow part of the periodic orbit being tangent to the take-off and touch-down curve. Because the construction performed in this thesis is quite different, something like that cannot be established right away.

Up till now, it was assumed that $s > 0$, this was motivated by the fact that this corresponds to a pattern traveling uphill. However, a priori this need not be the case[5]. For $s < 0$, the take-off and touch-down curves are symmetric around a line $p = su$ which is now on the left side of the u-axis, see figure 5.10. However, the stable and unstable manifolds $\ell^{s,u}$ are still symmetric around $p = c$. Also, since in the analysis above asymptotic methods were used it is not yet clear what happens when s becomes small, for example $\mathcal{O}(\varepsilon)$ or even $s = 0$.

5.4.1 Negative traveling wave speed

In this subsection it will be examined what happens when s is negative. It can be shown that no periodic orbits can exist for a negative s-value. This is due to the persisting symmetry in $\ell^{s,u}$ and will follow from a similar geometric approach as before.

In this case, the construction which was performed above is most conveniently applied to the backward flow. Note that for periodic orbits in (2.4), the orbit of $\mathcal{L}$ should be mapped into the same point by the Poincaré map for both forward and backward flow. A periodic orbit of (2.4) corresponds to a fixed point of $\mathcal{L}$. The construction is now the other way around because of the change in sign of s and therefore the change in the take-off and touch-down curves. However, in the construction for $s > 0$, the bifurcation point for existence of periodic orbits was determined by symmetry of the stable and unstable manifolds compared to the symmetry of the take-off and touch-down curves. Because $c > 0$, this can no longer be done in such a manner, because $p = su$ and $p = c$ no longer intersect for a positive u. Consequently, the configuration will the same for all $s < 0$ and will be either similar to figure 5.1 or similar to 5.7.

In this subsection it is given that $c > 0$ and $s < 0$. At the u-value which is determinative, define this u_1, the touch-down curve and stable manifold ℓ^s

[5] It should be positive because of biological interests, but mathematically there is no reason why s would not be negative.

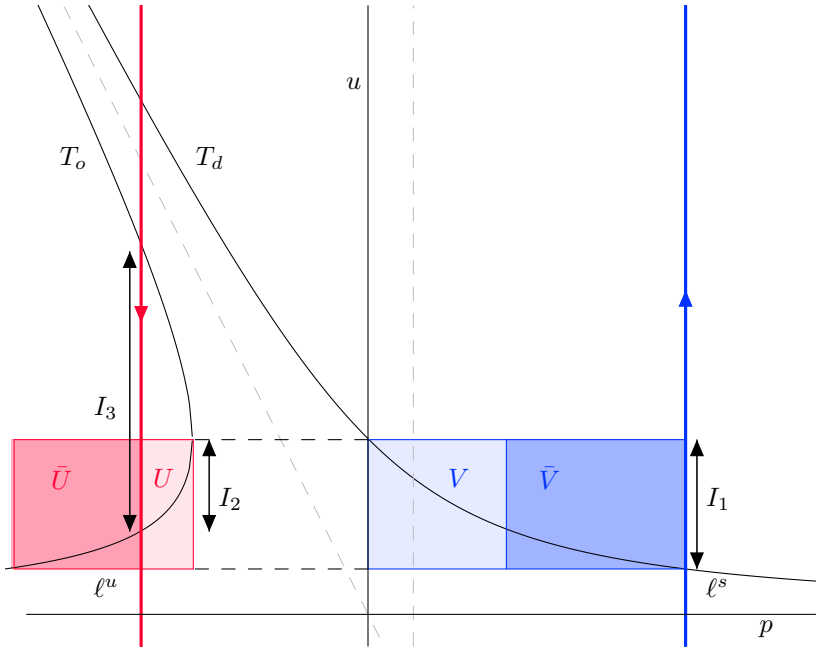

Figure 5.10: Schematic picture of $\mathcal{M}$ for $s < 0$. The orbits that take off at some point in $U \cap T_o$ will touch down at the corresponding value in $V \cap T_d$. The darker red area in U, $\bar{U}$ is the area where orbits from V are sent to in backwards fast scale, and that are mapped outside of $\mathcal{A}$.

intersect. At this point, the distance of ℓ^s is always smaller than the distance of ℓ^s to $p = su$. Because of the symmetry, this yields that ℓ^u at $u = u_1$ is always closer to $p = 0$ than the value of T_d at $u = u_1$. This means that the configuration of the phase plane is always as depicted in figure 5.10. As an analogue of lemma 1, it follows that no periodic orbits can exist.
The same iterative process can be performed, but now for backward 'time'[6]. This yields the same property, so all orbits starting in V will eventually be mapped outside of $\mathcal{A}$ in backward flow. Since periodic orbits in particular need to be bounded for both forward and backward flow, this implies that no periodic orbits can exist for $s < 0$.

5.4.2 Small traveling wave speed

Summarizing the results on periodic orbits yields that periodic orbits can exist neither for $su_1 > c$ nor for $s < 0$. These restrictions do give a sense about what could be the other boundary point of the range for which periodic orbits can exist; $s = 0$. However, this cannot be verified by the present $\mathcal{O}(1)$ approach. The analysis performed to give insight in the behavior of (2.4) used leading order approximations, see especially Remark 3.

For $0 < s \ll 1$, the take-off and touch-down curves are almost symmetric around the u-axis. The stable and unstable manifolds $\ell^{s,u}$ are symmetric around the line $p = c$. If, in addition to $0 < s \ll 1$, it is assumed that $0 < c \ll 1$, so a very flat hill, the unstable manifolds become almost symmetric around the u-axis.
This means that the situation becomes more and more similar to what is done in [3]. Then there can be a saddle node bifurcation where a periodic solution is

[6]Here, time is measured in ξ.

tangent to the take-off and touch-down curve. To determine this point, another leading order analysis needs to be performed. This will not be done in this thesis. A short outline is that first a new spatial variable needs to be introduced, such that the behavior can be studied even closer to the u-axis. Then, with asymptotic methods, the leading order behavior of the orbits in this domain can be determined, preferably in the form of level sets such that the same analysis as in [3] can be performed. However, the outcome will not be the same as in [3]. This is due to the asymmetry in $\ell^{s,u}$, which remains for $0 < s \ll 1$. One can expect that there will not be two families of periodic orbits that collide in a saddle-node bifurcation, but just one family of periodic orbits. This, but also the analysis for $0 < s \ll 1$ and $c = \mathcal{O}(1)$, needs further investigation.

Chapter 6

Conclusions and discussion

The aim of this thesis was to construct solutions of (1.4) which correspond to behavior that was observed in nature. As was explained in the introduction, periodic patterns in vegetation on hillsides tend to travel uphill as time passes. With the use of geometric singular perturbation theory, traveling pulse solutions of (1.4) were examined. The analysis that was performed, has provided insight in the behavior of these solutions. In this chapter, a short summary of the results will be presented and an overview of questions that arose during the research will be given.

6.1 Conclusions

In the first two chapters, a model describing the interplay between biomass and water infiltration was constructed. In chapter 1, it is explained what the ecological and biological meaning is of the terms that are included, and in chapter 2 this model was modified such that it was ready to use for geometric singular perturbation theory. This theory has been the framework of our analysis throughout the thesis.

In the third chapter, the leading order behavior of (2.4) was derived with the use of asysmptotic methods. Also, a Melnikov method has led us to the computation of the take-off and touch-down curves. The conclusions that could be drawn in this chapter have been the building blocks for the subsequent chapters.

In chapter four, the first main result was obtained. A existence theorem for homoclinic orbits in (2.4) was stated and proved. The proof was based on geometric properties of the phase space. In particular the stable and unstable manifolds and the take-off and touch-down curves. For every given $a, b, c > 0$ there exists exactly one wave speed s such that the system (2.4) possesses a homoclinic orbit. From a biological point of view this corresponds to an traveling oasis.

In the fifth and last chapter, periodic orbits were considered. By defining a special Poincaré map and Banach's fixed point theorem, the existence of periodic orbits was shown. For every c there exists a range of wave speeds s such that periodic orbits exist. For systems like (2.4), this approach had not been used before.
It was also shown that for wave speeds outside this range, no periodic orbits can be constructed. This has lead us to a bifurcation curve in s, c-space. Also two special cases where $s < 0$ or $0 < s \ll 1$ were studied. It was shown that for negative wave speeds, no periodic orbits can exist.

6.2 Further research suggestions

There are still many open questions concerning system (1.4). Some of these were derived from choices that were made in this thesis in order to perform a certain mathematical analysis. For example, the rescaling of (1.4) to (2.4) could be done in various ways. In this thesis on of the motivations for the rescaling was to obtain

a system to which geometric singular perturbation theory could be applied. Other approaches to this system could be valuable as well. In Chapter 1, it was assumed that $\gamma = 1$, i.e. linear diffusion in the U-equation. In the model suggested by Klausmeier, [7], the distinction between surface water (water on top of the surface) and soil water (water penetrated into the soil) is not explicitly made. An example to overcome this is to introduce a three-component system.
In [11] it is argued that linear diffusion is strongly simplified. A very good alternative would be $\gamma = 2$, which makes the U-equation nonlinear. The analysis of the saddle point P is then completely different.

Also, in the fifth chapter, we decide to not consider the explicit solutions of the periodic orbits. Since the slow reduced system is linear, this could very well lead to a more quantifying analysis of the periodic orbits.
Other questions originated from the results that were derived. A natural continuation of the proof of existence of both periodic and homoclinic orbits is whether or not these solutions are stable. This relates to the biological and ecological meaning of the system, because unstable solutions will never actually appear in the deserts. This is a big task that needs to be fulfilled such that the results that were obtained in this thesis can become very valuable to ecologists.
Also, no higher order analysis was done with respect to the changes in the system for $0 < s \ll 1$. This can be interesting, because a small value of s could be realistic. In the rescaling of (1.4) to (2.4), the parameter s was obtained such that it corresponds to small wave speeds (i.e. almost stationary solutions). However, it is not a priori clear that this is the correct rescaling. A study of the case where $0 < s \ll 1$ can be important.

Bibliography

[1] R.A. Adams, *Calculus, A complete course*, Sixth Edition, Pearson Addison Wesley, Toronto, (2006).

[2] A. Doelman et al, *Spatiallyl periodic and aperiodic multi-pulse patterns in the one-dimensional Gierer-Meinhardt equation*, Methods and Applications of Analysis, 8 (2001), pp.387-414.

[3] A. Doelman et al, *Pattern Formation in the one-dimensional Gray-Scott model*, Nonlinearity, 10 (1997), pp. 523-563.

[4] N. Fenichel, *Geometric singular perturbation theory for ordinary differential equations*, Journal of Diff. Eq., 31 (1979), pp. 53-98.

[5] J. Guckenheimer and P. Holmes, *Nonlinear Oscillations, Dynamical Systems, and Bifurcations of Vector Fields*, Springer-Verlag, New York, (1983).

[6] G. Hek, *Geometric singular perturbation theory in biological practice*, Journal for Mathematical Biology, 60 (2010), pp. 347-386.

[7] C.A. Klausmeier, *Regular and irregular patterns in semi-arid vegetation*, Science, 284 (1999), pp.1826-1828.

[8] W.A. Macfadyen, *Vegetation patterns in the semi-desert plains of British Somaliland*, The Geographical Journal, 116 (1950), pp. 199-211.

[9] M. Searcóid, *Metric Spaces*, Springer-Verlag, London, (2007).

[10] S. van der Stelt, *Rise and Fall of periodic patterns in a GKGS model*, PhD thesis, CWI (2012).

[11] S. van der Stelt, A. Doelman, G. Hek and J.D.M Rademacher, *Rise and Fall of periodic patterns for a GKGS model*, Journal of Nonlinear Science, DOI 10.1007/s00332-012-9139-0.